Title: Late-surviving New Mexican dinosaurs illuminate high end-Cretaceous diversity and provinciality

Authors: Andrew G. Flynn[1,2,3*], Stephen L. Brusatte[4,5†], Alfio Alessandro Chiarenza[6†], Jorge García-Girón[7,8†], Adam J. Davis[3,9‡], C. Will Fenley IV[3‡], Caitlin E. Leslie[3,10‡], Ross Secord[11‡], Sarah Shelley[4,12‡], Anne Weil[13,14‡], Matthew T. Heizler[15*], Thomas E. Williamson[5*], Daniel J. Peppe[3*].

Affiliations:
[1]Department of Geological Sciences, New Mexico State University, 1255 N. Horseshoe St., Las Cruces, NM, 88003
[2]Department of Paleobiology, National Museum of Natural History, Smithsonian Institution, 10th and Constitution Ave. NW, Washington, DC, 20013
[3]Terrestrial Paleoclimatology Research Group, Department of Geosciences, Baylor University, One Bear Place #97354, Waco, TX 76798-7354
[4]University of Edinburgh, School of GeoSciences, Grant Institute, James Hutton Road, Edinburgh EH9 3FE, UK
[5]New Mexico Museum of Natural History and Science, 1801 Mountain Road, NW, Albuquerque, NM 87104-1375, USA
[6]Department of Earth Sciences, University College London, Gower Street, London, WC1E 6BT
[7]Geography Research Unit, University of Oulu, P.O. Box 3000, FI-90014 Oulu, Finland
[8]Department of Biodiversity and Environmental Management, Universidad de León, Campus de Vegazana, 24007 León, Spain
[9]WSP USA Inc., 46850 Magellan Drive, Novi, MI, 48377
[10]ExxonMobil, 22777 Springwoods Village Parkway, Spring, Texas, 77389
[11]Department of Earth and Atmospheric Sciences, University of Nebraska-Lincoln, Lincoln, NE 68588-0340, USA
[12]Department of Life Sciences, University of Lincoln, Joseph Banks Laboratories, Green Lane, Lincoln LN6 7DL, UK
[13]Department of Anatomy and Cell Biology, Oklahoma State University Center for Health Sciences, Tulsa, OK, USA, 74107
[14]Sam Noble Museum of Natural History, 2401 Chautauqua Ave., Norman, OK, 73072
[15]New Mexico Bureau of Geology and Mineral Resources, 801 Leroy Place, Socorro NM, 87801
[†]These authors contributed equally to this work and are listed alphabetically.
[‡]These authors contributed equally to this work and are listed alphabetically.
*Correspondence to: agflynn@nmsu.edu, matt.heizler@nmt.edu, thomas.williamson@dca.nm.gov, daniel_peppe@baylor.edu

Abstract:

It has long been debated whether non-avian dinosaurs went extinct abruptly or gradually at the end-Cretaceous (66 million years ago), because their fossil record at this time is mostly limited to northern North America. We constrain a dinosaur-rich unit to the south, the Naashoibito Member in New Mexico, to the very latest Cretaceous (~66.4–66.0 myr) preserving some of the last-known non-avian dinosaurs. Ecological modeling shows that North American terrestrial vertebrates maintained high diversity and endemism in the latest Cretaceous and early Paleogene, with bioprovinces shaped by temperature and geography. This counters the notion of a low-diversity cross-continental fauna and suggests dinosaurs were diverse and partitioned into regionally distinct assemblages during the final few hundred thousand years before the end-Cretaceous asteroid impact.

Main Text:

Introduction

The most iconic mass extinction in Earth history occurred at the Cretaceous–Paleogene (K–Pg) boundary, 66.052 ± 0.008 Million years ago (Ma) (*1*), as rapid environmental destruction led to the death of around 75% of species, most famously the non-avian dinosaurs, and subsequently restructured terrestrial ecosystems (e.g., *2–5*). An asteroid impacted Earth at the end of the Cretaceous (*6*, *7*), synchronous with the Cretaceous–Paleogene boundary and the main pulse of extinction (*8*). The most voluminous episode of Deccan trap volcanism also occurred within a small time window just before and after the boundary (e.g., *9–11*). Ecological and climate models suggest the asteroid impact, and not volcanism, was the main driver of extinction in the marine realm (e.g., *12*), although the tempo and mode of extinction in terrestrial ecosystems are less clear. Debate centers on whether dinosaurs, in particular, vanished abruptly while diverse and flourishing (e.g., *13–16*), or were in long-term decline before the end-Cretaceous (*17*, *18*).

This uncertainty stems from a bias in the geological record: the only well-sampled and temporally constrained terrestrial faunas straddling the K–Pg boundary come from the northern Great Plains of North America (e.g., *19*). There, the Hell Creek and Fort Union Formations (and equivalents) document a seemingly abrupt extinction of non-avian dinosaurs and rapid establishment of mammalian faunas within a few tens of thousands of years (*1*, *13*, *20–24*). It is uncertain, however, whether this is a local, regional, or global pattern. These terminal Cretaceous records are part of a larger sequence of faunas across the ancient continent of Laramidia—now western North America— spanning the final ~15 million years of the Cretaceous (Campanian and Maastrichtian ages). Dinosaurs from these faunas have been well studied for over a century and include canonical species like carnivorous tyrannosaurids, horned ceratopsians, and duck-billed hadrosaurs.

There is a notion that the Campanian (83.6–72.1 Ma) was a time of high regional diversity and endemism in Laramidia, underlain by a general division into northern and southern bioprovinces (*25–29*). In contrast, the Maastrichtian (72.1–66.0 Ma) is held to have been more uniform, with a cosmopolitan dinosaur assemblage spanning the continent (*30*, *31*). Ecological restructuring, from Campanian provinciality to Maastrichtian homogeneity, is associated with a hypothesized prolonged decline of non-avian dinosaurs, increasing their susceptibility to extinction (*31*). How to best test the existence of provinciality, and its causes, remains contentious and requires integrating fossil and climatic records (*32*), understanding sampling biases (*33*, *34*), and well-constrained fossil localities from the latest Cretaceous (*35*). Especially troublesome is the lack of well-sampled terminal Cretaceous dinosaur assemblages from southern Laramidia. In their absence, it is difficult to understand the distribution and structure of the last dinosaur-dominated ecosystems before the K–Pg boundary (*36*).

The San Juan Basin of New Mexico, ~1,500 kilometers south of classic sites in the northern Great Plains, has yielded a wealth of fossils collected since the mid-late 1800s (Fig. 1A-B) (see *37*). These include dinosaur assemblages from the Campanian Fruitland and Kirtland Formations (ca. 75.17–73.50 Ma; *(38)*), and mammals in the Nacimiento Formation, one of the world's best records of early Paleocene evolution after the extinction (ca. 65.7 to 62.3 Ma) (*39*, *40*). What the San Juan Basin seemed to lack, however, are fossils from the terminal Cretaceous. The "Alamo Wash local fauna" from the Naashoibito Member of the Kirtland Formation (*41*) documents the last known non-avian dinosaurs in New Mexico (Fig. 1), but its age has been controversial. It has typically been considered early to middle Maastrichtian based on faunal comparisons to other, better constrained Laramidian assemblages (*42*), with the most recent geochronological revisions placing it at ca. 70 Ma

(*35*). However, the lack of independent depositional age constraints has led to uncertainty about its numerical age (*41*).

We provide a new look at the last-surviving dinosaur-dominated ecosystems, by presenting a revised geochronology of the Naashoibito Member—demonstrating it is latest Maastrichtian and preserves dinosaurs from the very end-Cretaceous—and ecological analyses to test whether there were changes in faunal provinciality during the latest Cretaceous and into the Paleogene.

Age of uppermost Cretaceous deposits within the San Juan Basin

The Naashoibito Member of the Kirtland Formation (= Naashoibito Member of the Ojo Alamo Formation in (*43*)) is exposed in the western San Juan Basin and consists of ~30 m of fluvial deposits (*44*, *45*). The Naashoibito unconformably overlies the upper Campanian De-Na-Zin Member of the Kirtland and Fruitland Formations (75.166 ± 0.014 to 73.496 ± 0.039 Ma (*38*)) and unconformably underlies the earliest Paleocene Ojo Alamo Sandstone (~66.0 – 65.7 Ma (*40, 46*)). The age of the Naashoibito—and its latest Cretaceous dinosaurs—is contentious, with previous work suggesting a middle Maastrichtian age (~70-69 Ma) based on the presence of the sauropod *Alamosaurus* and lambeosaurine hadrosaurs, both absent in the latest Maastrichtian of the northern Great Plains (*35*, *36*, *47*, *48*), while other workers have argued that the dinosaurs and mammals are more characteristic of a latest Maastrichtian age (~67-66 Ma) (*41*, *49–51*). Finally, Fassett et al. (*52, 53*) proposed that the Naashoibito is Paleocene based on reinterpretations of previously published palynology and U-Pb dating of a dinosaur bone, but this has been consistently refuted (*47*, *54*, *55*). We combined detrital-sanidine geochronology and magnetostratigraphy to constrain the age of the Naashoibito and its fossil assemblages.

Five lithostratigraphic sections were measured, and correlated to generate a composite litho- and magnetostratigraphic section (Figs. 1B-C, S1), and then combined with previous work from the overlying Paleocene Ojo Alamo Sandstone and lower Nacimiento Formation to generate an uppermost Cretaceous through lower Paleocene chronology (Fig. 1C). We conducted detrital sanidine $^{40}Ar/^{39}Ar$ geochronology on grains from two dinosaur bone-bearing Naashoibito localities (*n = 1046*) (Tables S7 – S11), with 491 crystals yielding dates less than 75 Ma (Fig. 1D; see supplement for full details). Samples H08-Sand-08 and SJ-SS-bone were collected ~20.0 m below the Naashoibito-Ojo Alamo contact and ~5 m above the base of the Naashoibito (Fig. 1C). H08-Sand-08 yields a maximum depositional age (MDA) of 66.87 ± 0.04 Ma derived from a normal distribution (mean squared weight deviation (MSWD) = 1.54) of eight crystals (Fig. 1D) while sample SJ-SS-Bone did not yield grains less than 70 Ma (MDA = 72.61 ± 0.21 Ma). Sample H13-SJ-14 is directly from the dinosaur-bearing "34-Bone Site" approximately 3.5 m above the base of the Naashoibito Member (*56*), which contains the partial skeleton of a lambeosaurine hadrosaur. The MDA of the H13-SJ-13 sample, based on the two youngest grains, is 66.38 ± 0.08 Ma (Fig, 1D; Tables S7-S11). Thus, we have identified two dinosaur fossil-bearing samples that are late Maastrichtian, with H13-SJ-13 isotopically dated to be less than 400 Kyr from the K-Pg boundary.

The magnetostratigraphic analyses from this study identified two local polarity zones within our section: 1) A+ at the base of the Naashoibito Member and 2) B- which incorporates the upper Naashoibito Member, entire Ojo Alamo Sandstone, and basal Nacimiento Formation (Fig. 1C, Table S2). The MDAs of samples H13-SJ-14 (66.38 ± 0.08 Ma) and H08-Sand-08 (66.87 ± 0.04 Ma) constrain local polarity zones A+ and B- to magnetochrons C30n and C29r, respectively, of the Geomagnetic Polarity Timescale (GPTS) (cf., *57*). Thus, the major Naashoibito Member dinosaur bearing horizons are constrained to within 340 Kyr of the K-Pg boundary (Fig. 1C), contemporaneous with the Hell Creek fauna further north, and the Naashoibito fauna is separated from the earliest Paleocene Nacimiento

fauna by ~700 Kyr (Fig. 1C-D). Lastly, we identified an interval of normal polarity (from ~10-20 m; Fig. 1C) that previous work had erroneously correlated with a Cretaceous normal polarity chron *(58)* but our new analyses indicate that this is a zone of significant diagenetically overprinted reversed polarity (see Supplement for full discussion; Fig. S4).

Latest Cretaceous and early Paleocene faunal provinciality

It has long been debated whether North American Campanian-Maastrichtian vertebrates had provincial or more uniform distributions (*25-29*), if the degree of provinciality decreased towards the end of the Cretaceous (*30-31, 59-61*), and which geographic or climatic factors were most responsible for such patterns (*62*). Much previous work was qualitative, and depended on interpretation of a biased fossil record or observed distribution of a few species (e.g., *Tyrannosaurus*, *Alamosaurus*) rather than entire faunas.

We applied multivariate and resemblance-based methods from metacommunity ecology and biogeography (e.g., *63–66*) on a dataset of terrestrial and fluvio-lacustrine vertebrates to assess whether there was faunal provinciality during the latest Cretaceous and earliest Paleocene, and if so, what underpinned it. We identified two optimal bioprovinces in each interval (Campanian, Maastrichtian, Danian) using *k*-means clustering (Figs. 2-3, S8; Table S12), which held after controlling for finer biozone-level binning strategies (Tables S13-S14), and bootstrap resampling to account for fossil record and dataset biases (Fig. S9). When analyzed individually, dinosaurs were separated into two bioprovinces across all latest Cretaceous time intervals, whereas mammals formed two bioprovinces in the Campanian, a single cosmopolitan fauna in the Maastrichtian, and separated again after the extinction (Figs. 3, S8; Tables S12-13, S15). Overall, these findings indicate large-scale faunal provinciality during the Campanian and Maastrichtian that was maintained across the K–Pg boundary into the Danian (Figs. 2-3).

Bioprovinces were significantly different in mean assemblage composition in the Late Cretaceous and early Paleogene (Figs. 2-3; Tables S16-S19), although they did not differ in their amount of internal variation (spatial beta diversity within each province: *67-69*) across this interval (Tables S20-S23). Different taxa (Figs. 2-3) characterized the different provinces over time (Tables S24-S28). Discriminant analysis of principal components on environmental and paleogeographic factors (elevation, latitude, longitude, temperature, mean and seasonal precipitation: *70-73*) indicate that provinciality was largely controlled by temperature in the Cretaceous, with spatial location having a notable role after the extinction (Fig. S12). Thus, thermal constraints were most instrumental in explaining the bioprovinces, not strictly north-south geographic separation, although geography played a secondary role.

Discussion

Our geochronology for the Naashoibito Member shows that its dinosaurs and other fossils are latest Maastrichtian and contemporaneous with the Hell Creek faunas to the north (e.g., *23*, *35*). The last-sampled dinosaurs of the Naashoibito persisted into C29r, the final subdivision of the Cretaceous polarity timescale (*54*), and lived within ~340,000 years of the K–Pg boundary and likely endured until the boundary, as in the Hell Creek area. The Naashoibito dinosaurs include a variety of species spanning major groups, sizes, and dietary categories, and do not appear abnormal or depauperate compared to earlier faunas (*16*), suggesting dinosaurs were thriving in New Mexico until the end of the Cretaceous.

Our ecological analyses (*74*, *75*) show that the distribution of terrestrial and fluvio-lacustrine vertebrates on Laramidia was characterized by elevated provinciality in the Campanian, as long recognized (e.g., *25–29*, *31*) and that provinciality continued into the

Maastrichtian, which was acknowledged in earlier studies (e.g., *26*, *27*), but called into question by recent work (*30*, *31*, *36*). This counters the prevailing idea that Laramidian Maastrichtian faunas were largely uniform, with low spatial beta diversity (*30*, *31*), implicated as a factor to the dinosaur extinction, because a low-diversity, cosmopolitan fauna is potentially more susceptible to collapse than one with a greater variety of species subdividing habitats (*31*). Instead, we recognize the final ca. one million years of dinosaur evolution as a time of biogeographic diversity and partitioning among terrestrial faunas in western North America.

Our analyses further suggest that temperature was instrumental to these faunal separations. While traditional views attributed faunal differences to strict north-south geographic boundaries (*29*), recent advances have suggested that abiotic factors, particularly temperature, also played a role (*76–80*). Among herbivores, warmer regions may have been more tolerable for sauropods (southwestern North America (*76*)), while the cooler, more temperate regions (modern Great Plains) may have been more suitable for hadrosaurines (*81–83*). Our results challenge the notion of straightforward geographic boundaries as the primary driver of faunal differences and highlight the significance of abiotic factors in fostering heterogeny of dinosaur-dominated ecosystems prior to the K–Pg extinction.

This picture is still a North American one. Fossils of well-dated terminal Cretaceous vertebrates are rare elsewhere, and have yet to be confidently dated with radioisotopic methods, but there is an emerging signal that dinosaur ecosystems were robust during the end-Cretaceous. Although not as accurately dated as the Hell Creek and Naashoibito—and not able to be studied with our quantitative ecology techniques yet—growing evidence indicates dinosaurs also survived into C29r (last ~340 Kyr of the Cretaceous) in Europe and South America (*84–86*). These are all diverse faunas, with an array of herbivores and carnivores, occupying a range of body sizes, belonging to major groups such as theropods, sauropods, and ornithischians. Thus, we argue that the sum of evidence suggests that non-avian dinosaurs were abruptly struck down at the end of the Cretaceous (*4*, *14*, *16*) and were not in long-term decline (*18*)

Mammals rapidly diversified after the end-Cretaceous extinction in northern and southern Laramidia (*8*, *37*). The early mammalian ‘recovery’ faunas of the Puercan 2 (Pu2) biozone first appear in the San Juan Basin within ~300 kyr of the K–Pg boundary (*39*). Compared with the preceding latest Cretaceous, these faunas were more taxonomically diverse, exhibiting a much greater range of diets and body size, and include many placental mammals, some on the evolutionary line to modern groups (*37*). Turnover was high, as Pu2 lasted less than 425 kyr before giving way to the Puercan 3 (Pu3) assemblage (*40*). Meanwhile, regional faunal differences between north and south, and the temperature gradient that characterized the Cretaceous, persisted into the Paleogene (*32*, *46*), demonstrating the extinction did not homogenize faunas in its aftermath. The rapid pace of mammalian recovery and diversification contrasts with languid recovery after the end-Permian extinction, when it took several million years for new terrestrial vertebrates (such as proto-dinosaurs) to seize niches and ecosystems to stabilize (*87*, *89*, *90*). The end-Cretaceous extinction of dinosaurs was sudden, but then swiftly afterward mammals began their rise.

References and Notes

1. C. J. Sprain, P. R. Renne, W. A. Clemens, G. P. Wilson, Calibration of chron C29r: New high-precision geochronologic and paleomagnetic constraints from the Hell Creek region, Montana. *GSA Bull.* **130**, 1615–1644 (2018).

2. N. MacLeod, P. F. Rawson, P. L. Forey, F. T. Banner, M. K. Boudagher-Fadel, P. R. Bown, J. A. Burnett, P. Chambers, S. Culver, S. E. Evans, C. Jeffery, M. A. Kaminski,

A. R. Lord, A. C. Milner, A. R. Milner, N. Morris, E. Owen, B. R. Rosen, A. B. Smith, P. D. Taylor, E. Urquhart, J. R. Young, The Cretaceous-Tertiary biotic transition. *J. Geol. Soc.* **154**, 265–292 (1997).

3. J. D. Archibald, *Extinction and Radiation: How the Fall of Dinosaurs Led to the Rise of Mammals* (JHU Press, 2011).

4. S. L. Brusatte, R. J. Butler, P. M. Barrett, M. T. Carrano, D. C. Evans, G. T. Lloyd, P. D. Mannion, M. A. Norell, D. J. Peppe, P. Upchurch, T. E. Williamson, The extinction of the dinosaurs. *Biol. Rev.* **90**, 628–642 (2015).

5. A. A. Chiarenza, S. L. Brusatte, "Dinosaurs, Extinction Theories for" in *Encyclopedia of Biodiversity (Third Edition)*, S. M. Scheiner, Ed. (Academic Press, Oxford, 2023), pp. 298–309.

6. L. W. Alvarez, W. Alvarez, F. Asaro, H. V. Michel, Extraterrestrial cause for the Cretaceous-Tertiary extinction: experimental results and theoretical interpretation. *Science* **208**, 1095 (1980).

7. P. Schulte, L. Alegret, I. Arenillas, J. A. Arz, P. J. Barton, P. R. Bown, T. J. Bralower, G. L. Christeson, P. Claeys, C. S. Cockell, G. S. Collins, A. Deutsch, T. J. Goldin, K. Goto, J. M. Grajales-Nishimura, R. A. F. Grieve, S. P. S. Gulick, K. R. Johnson, W. Kiessling, C. Koeberl, D. A. Kring, K. G. MacLeod, T. Matsui, J. Melosh, A. Montanari, J. V. Morgan, C. R. Neal, D. J. Nichols, R. D. Norris, E. Pierazzo, G. Ravizza, M. Rebolledo-Vieyra, W. U. Reimold, E. Robin, T. Salge, R. P. Speijer, A. R. Sweet, J. Urrutia-Fucugauchi, V. Vajda, M. T. Whalen, P. S. Willumsen, The Chicxulub Asteroid Impact and Mass Extinction at the Cretaceous-Paleogene Boundary. *Science* **327**, 1214–1218 (2010).

8. P. R. Renne, F. J. Hilgen, D. F. Mark, J. Smit, R. Mundil, A. L. Deino, W. S. Mitchell III, K. F. Kuiper, L. Morgan, Time scales of critical events around the Cretaceous-Paleogene boundary. *Science* **339**, 684–687 (2013).

9. T. S. Tobin, G. P. Wilson, J. M. Eiler, J. H. Hartman, Environmental change across a terrestrial Cretaceous-Paleogene boundary section in eastern Montana, USA, constrained by carbonate clumped isotope paleothermometry. *Geology* **42**, 351–354 (2014).

10. B. Schoene, M. P. Eddy, K. M. Samperton, C. B. Keller, G. Keller, T. Adatte, S. F. R. Khadri, U-Pb constraints on pulsed eruption of the Deccan Traps across the end-Cretaceous mass extinction. *Science* **363**, 862–866 (2019).

11. C. J. Sprain, P. R. Renne, L. Vanderkluysen, K. Pande, S. Self, T. Mittal, The eruptive tempo of Deccan volcanism in relation to the Cretaceous-Paleogene boundary. *Science* **363**, 866–870 (2019).

12. P. M. Hull, A. Bornemann, D. E. Penman, M. J. Henehan, R. D. Norris, P. A. Wilson, P. Blum, L. Alegret, S. J. Batenburg, P. R. Bown, T. J. Bralower, C. Cournede, A. Deutsch, B. Donner, O. Friedrich, S. Jehle, H. Kim, D. Kroon, P. C. Lippert, D. Loroch, I. Moebius, K. Moriya, D. J. Peppe, G. E. Ravizza, U. Röhl, J. D. Schueth, J. Sepúlveda, P. F. Sexton, E. C. Sibert, K. K. Śliwińska, R. E. Summons, E. Thomas, T.

Westerhold, J. H. Whiteside, T. Yamaguchi, J. C. Zachos, On impact and volcanism across the Cretaceous-Paleogene boundary. *Science* **367**, 266–272 (2020).

13. D. A. Pearson, T. Schaefer, K. R. Johnson, D. J. Nichols, J. P. Hunter, "Vertebrate biostratigraphy of the Hell Creek Formation" in *The Hell Creek Formation and the Cretaceous-Tertiary Boundary in the Northern Great Plains: An Integrated Continental Record of the End of the Cretaceous*, J. H. Hartman, K. R. Johnson, D. J. Nichols, Eds. (Geological Society of America Special Paper 361, Boulder, CO, 2002), pp. 145–167.

14. A. A. Chiarenza, P. D. Mannion, D. J. Lunt, A. Farnsworth, L. A. Jones, S.-J. Kelland, P. A. Allison, Ecological niche modelling does not support climatically-driven dinosaur diversity decline before the Cretaceous/Paleogene mass extinction. *Nat. Commun.* **10**, 1091 (2019).

15. A. A. Chiarenza, A. Farnsworth, P. D. Mannion, D. J. Lunt, P. J. Valdes, J. V. Morgan, P. A. Allison, Asteroid impact, not volcanism, caused the end-Cretaceous dinosaur extinction. *Proc. Natl. Acad. Sci.* **117**, 17084–17093 (2020).

16. J. García-Girón, A. A. Chiarenza, J. Alahuhta, D. G. DeMar, J. Heino, P. D. Mannion, T. E. Williamson, G. P. Wilson Mantilla, S. L. Brusatte, Shifts in food webs and niche stability shaped survivorship and extinction at the end-Cretaceous. *Sci. Adv.* **8**, eadd5040 (2022).

17. M. Sakamoto, M. J. Benton, C. Venditti, Dinosaurs in decline tens of millions of years before their final extinction. *Proc. Natl. Acad. Sci.* **113**, 5036–5040 (2016).

18. F. L. Condamine, G. Guinot, M. J. Benton, P. J. Currie, Dinosaur biodiversity declined well before the asteroid impact, influenced by ecological and environmental pressures. *Nat. Commun.* **12**, 3833 (2021).

19. D. E. Fastovsky, A. Bercovici, The Hell Creek Formation and its contribution to the Cretaceous–Paleogene extinction: A short primer. *Cretac. Res.* **57**, 368–390 (2016).

20. J. A. Lillegraven, J. J. Eberle, Vertebrate Faunal Changes through Lancian and Puercan Time in Southern Wyoming. *J. Paleontol.* **73**, 691–710 (1999).

21. D. A. Pearson, T. Schaefer, K. R. Johnson, D. J. Nichols, Palynologically calibrated vertebrate record from North Dakota consistent with abrupt dinosaur extinction at the Cretaceous-Tertiary boundary. *Geology* **29**, 39–42 (2001).

22. G. P. Wilson, "Mammalian extinction, survival, and recovery dynamics across the Cretaceous-Paleogene boundary in northeastern Montana, USA" in *Through the End of the Cretaceous in the Type Locality of the Hell Creek Formation in Montana and Adjacent Areas*, G. P. Wilson, W. A. Clemens, J. R. Horner, J. H. Hartman, Eds. (Geological Society of America Special Paper 503, 2014), pp. 365–392.

23. C. J. Sprain, P. R. Renne, G. P. Wilson, W. A. Clemens, High-resolution chronostratigraphy of the terrestrial Cretaceous-Paleogene transition and recovery interval in the Hell Creek region, Montana. *GSA Bull.* **127**, 393–409 (2015).

24. T. R. Lyson, I. M. Miller, A. D. Bercovici, K. Weissenburger, A. J. Fuentes, W. C. Clyde, J. W. Hagadorn, M. J. Butrim, K. R. Johnson, R. F. Fleming, R. S. Barclay, S. A. Maccracken, B. Lloyd, G. P. Wilson, D. W. Krause, S. G. B. Chester, Exceptional continental record of biotic recovery after the Cretaceous–Paleogene mass extinction. *Science* **366**, 977-983 (2019).

25. R. E. Sloan, Cretaceous and Paleocene terrestrial communities of Western North America. *Proc North Am Paleont Conv. Chic.* **1969**, 427–453 (1970).

26. T. M. Lehman, Late Maastrichtian paleoenvironments and dinosaur biogeography in the western interior of North America. *Palaeogeogr. Palaeoclimatol. Palaeoecol.* **60**, 189–217 (1987).

27. T. M. Lehman, "Late Cretaceous Dinosaur Provinciality" in *Mesozoic Vertebrate Life*, D. H. Tanke, K. Carpenter, Eds. (Indiana University Press, Bloomington, IN, 2001), pp. 310–328.

28. S. D. Sampson, M. A. Loewen, A. A. Farke, E. M. Roberts, C. A. Forster, J. A. Smith, A. L. Titus, New Horned Dinosaurs from Utah Provide Evidence for Intracontinental Dinosaur Endemism. *PLOS ONE* **5**, e12292 (2010).

29. T. A. Gates, A. Prieto-Márquez, L. E. Zanno, Mountain Building Triggered Late Cretaceous North American Megaherbivore Dinosaur Radiation. *PLOS ONE* **7**, e42135 (2012).

30. M. J. Vavrek, H. C. E. Larsson, Low beta diversity of Maastrichtian dinosaurs of North America. *Proc. Natl. Acad. Sci.* **107**, 8265–8268 (2010).

31. J. S. Mitchell, P. D. Roopnarine, K. D. Angielczyk, Late Cretaceous restructuring of terrestrial communities facilitated the end-Cretaceous mass extinction in North America. *Proc. Natl. Acad. Sci.* **109**, 18857–18861 (2012).

32. L. Burgener, E. Hyland, B. J. Reich, C. Scotese, Cretaceous climates: Mapping paleo-Köppen climatic zones using a Bayesian statistical analysis of lithologic, paleontologic, and geochemical proxies. *Palaeogeogr. Palaeoclimatol. Palaeoecol.* **613**, 111373 (2023).

33. C. D. Dean, A. A. Chiarenza, S. C. R. Maidment, Formation binning: a new method for increased temporal resolution in regional studies, applied to the Late Cretaceous dinosaur fossil record of North America. *Palaeontology* **63**, 881–901 (2020).

34. S. C. R. Maidment, C. D. Dean, R. I. Mansergh, R. J. Butler, Deep-time biodiversity patterns and the dinosaurian fossil record of the Late Cretaceous Western Interior, North America. *Proc. R. Soc. B Biol. Sci.* **288**, 20210692 (2021).

35. D. W. , Revised geochronology, correlation, and dinosaur stratigraphic ranges of the Santonian-Maastrichtian (Late Cretaceous) formations of the Western Interior of North America. *PLOS ONE* **12**, e0188426 (2017).

36. S. G. Lucas, R. M. Sullivan, A. J. Lichtig, S. G. Dalman, S. E. Jasinski, Late Cretaceous Dinosaur Biogeography and Endemism in the Western Interior Basin, North America: a Critical Re-evaluation. *N. M. Mus. Nat. Hist. Sci. Bull.* **71**, 195–214 (2016).

37. T. E. Williamson, The beginning of the age of mammals in the San Juan Basin, New Mexico: Biostratigraphy and evolution of Paleocene mammals of the Nacimiento Formation. *N. M. Mus. Nat. Hist. Sci. Bull.* **8**, 1–141 (1996).

38. J. Ramezani, T. L. Beveridge, R. R. Rogers, D. A. Eberth, E. M. Roberts, Calibrating the zenith of dinosaur diversity in the Campanian of the Western Interior Basin by CA-ID-TIMS U–Pb geochronology. *Sci. Rep.* **12**, 16026 (2022).

39. C. E. Leslie, D. Peppe, T. Williamson, M. Heizler, R. Secord, T. Leggett, High-resolution magnetostratigraphy of the upper Nacimiento Formation, San Juan Basin, New Mexico, USA: implications for basin evolution and mammalian turnover. *Am. J. Sci.* **318**, 300–334 (2018).

40. A. G. Flynn, A. J. Davis, T. E. Williamson, M. Heizler, C. W. Fenley IV, C. E. Leslie, R. Secord, S. L. Brusatte, D. J. Peppe, Early Paleocene Magnetostratigraphy and Revised Biostratigraphy of the Ojo Alamo Sandstone and Lower Nacimiento Formation, San Juan Basin, New Mexico, USA. *GSA Bull.* **132**, 2154–2174 (2020).

41. T. M. Lehman, "The Alamo Wash Local Fauna: a New Look at the Old Ojo Alamo Fauna" in *Advances in San Juan Paleontology*, S. G. Lucas, J. K. Jr. Rigby, B. S. Kues, Eds. (University of New Mexico Press, Albuquerque, NM, 1981), pp. 189–221.

42. R. M. Sullivan, S. G. Lucas, The Kirtlandian, a new land vertebrate "age" for the Late Cretaceous of Western North America. *Guideb. N. M. Geol. Soc.* **54**, 369–377 (2006).

43. R. M. Sullivan, S. G. Lucas, D. R. Braman, Dinosaurs, pollen, and the Cretaceous-Tertiary boundary in the San Juan Basin. *Guideb. N. M. Geol. Soc.* **56**, 395–407 (2005).

44. T. M. Lehman, Depositional environments of the Naashoibito Member of the Kirtland Shale, Upper Cretaceous, San Juan Basin, New Mexico. *N. M. Bur. Mines Miner. Resour. Circ.* **195**, 55–79 (1985).

45. L. H. Tanner, S. G. Lucas, Record of palaeoclimate across the Cretaceous–Palaeogene boundary from palaeosols in the west-central San Juan Basin, New Mexico, USA. *Depositional Rec.* **9**, 1131–1152 (2023).

46. A. G. Flynn, D. J. Peppe, Early Paleocene tropical forest from the Ojo Alamo Sandstone, San Juan Basin, New Mexico, USA. *Paleobiology* **45**, 612–635 (2019).

47. S. G. Lucas, R. M. Sullivan, S. M. Cather, S. E. Jasinski, D. W. Fowler, A. B. Heckbert, J. A. Spielmann, A. P. Hunt, No Definitive Evidence of Paleocene Dinosaurs in the San Juan Basin. *Palaeontol. Electron.* **12**, 1–10 (2009).

48. S. E. Jasinski, R. M. Sullivan, S. G. Lucas, Taxonomic Composition of the Alamo Wash Local Fauna from the Upper Cretaceous Ojo Alamo Formation (Naashoibito Member), San Juan Basin, New Mexico. *N. M. Mus. Nat. Hist. Sci. Bull.* **53**, 216–273 (2011).

49. T. M. Lehman, The multituberculate *Essonodon browni* from the Upper Cretaceous Naashoibito Member of the Kirtland Shale, San Juan Basin, New Mexico. *J. Vertebr. Paleontol.* **4**, 602–603 (1984).

409 50. T. E. Williamson, A. Weil, Metatherian Mammals from the Naashoibito Member,
410 Kirtland Formation, San Juan Basin, New Mexico and Their Biochronologic and
411 Paleobiogeographic Significance. *J. Vertebr. Paleontol.* **28**, 803–815 (2008).

412 51. T. E. Williamson, A. Weil, Stratigraphic Distribution of Sauropods in the Upper
413 Cretaceous of the San Juan Basin, New Mexico, with Comments on North America's
414 Cretaceous "Sauropod Hiatus." *J. Vertebr. Paleontol.* **28**, 1218–1223 (2008).

415 52. J. E. Fassett, R. A. Zielinski, J. R. Budahn, Dinosaurs that did not die: Evidence for
416 Paleocene dinosaurs in the Ojo Alamo Sandstone, San Juan Basin, New Mexico. *Geol.*
417 *Soc. Am. Spec. Pap.* **356**, 307–336 (2002).

418 53. J. E. Fassett, New geochronologic and stratigraphic evidence confirms the Paleocene
419 age of the dinosaur-bearing Ojo Alamo Sandstone and Animas Formation in the San
420 Juan Basin, New Mexico and Colorado. *Palaeontol. Electron.* **12**, 146 (2009).

421 53. A. E. Koenig, S. G. Lucas, L. A. Neymark, A. B. Heckert, R. M. Sullivan, S. E. Jasinski,
422 D. W. Fowler, Direct U-Pb dating of Cretaceous and Paleocene dinosaur bones, San
423 Juan Basin, New Mexico: COMMENT. *Geology* **40**, e262 (2012).

424 54. P. R. Renne, M. B. Goodwin, Direct U-Pb dating of Cretaceous and Paleocene dinosaur
425 bones, San Juan Basin, New Mexico: COMMENT. *Geology* **40**, e259 (2012).

426 55. A. P. Hunt, S. G. Lucas, An associated Maastrichtian hadrosaur and a Turonian
427 ammonite from the Naashoibito Member, Kirtland Formation (Late Cretaceous:
428 Maastrichtian), northwestern New Mexico. *N. M. J. Sci.* **31**, 27–35 (1991).

429 57. J. G. Ogg, "Geomagnetic Polarity Time Scale" in *Geologic Time Scale 2020*, F. M.
430 Gradstein, J. G. Ogg, M. D. Schmitz, G. M. Ogg, Eds. (Elsevier, 2020), pp. 159–192.

431 58. R. F. Butler, E. H. Lindsay, L. L. Jacobs, N. M. Johnson, Magnetostratigraphy of the
432 Cretaceous-Tertiary boundary in the San Juan Basin, New Mexico. *Nature* **267**, 318–
433 323 (1977).

434 59. J. R. Horner, M. B. Goodwin, N. Myhrvold, Dinosaur Census Reveals Abundant
435 Tyrannosaurus and Rare Ontogenetic Stages in the Upper Cretaceous Hell Creek
436 Formation (Maastrichtian), Montana, USA. *PLOS ONE* **6**, e16574 (2011).

437 60. M. A. Loewen, R. B. Irmis, J. J. W. Sertich, P. J. Currie, S. D. Sampson, Tyrant
438 Dinosaur Evolution Tracks the Rise and Fall of Late Cretaceous Oceans. *PLOS ONE* **8**,
439 e79420 (2013).

440 61. D. E. Fastovsky, Y. Huang, J. Hsu, J. Martin-McNaughton, P. M. Sheehan, D. B.
441 Weishampel, Shape of Mesozoic dinosaur richness. *Geology* **32**, 877–880 (2004).

442 62. K. Berry, Paleontological Evidence Against a Major Geographic Barrier at about the
443 Paleolatitude of Colorado, USA, during the Late Campanian (Late Cretaceous): The
444 Conspicuous Absence of Endemic Subclades of Chasmosaurine Ceratopsid (Horned)
445 Dinosaurs and Its Significance. *Mt. Geol.* **55**, 5–18 (2018).

63. T. Gonçalves-Souza, G. Q. Romero, K. Cottenie, Metacommunity versus Biogeography: A Case Study of Two Groups of Neotropical Vegetation-Dwelling Arthropods. *PLOS ONE* **9**, e115137 (2014).

64. J. Heino, J. Soininen, J. Alahuhta, J. Lappalainen, R. Virtanen, Metacommunity ecology meets biogeography: effects of geographical region, spatial dynamics and environmental filtering on community structure in aquatic organisms. *Oecologia* **183**, 121–137 (2017).

65. T. Leboucher, J. Tison-Rosebery, W. R. Budnick, A. Jamoneau, W. Vyverman, J. Soininen, S. Boutry, S. I. Passy, A metacommunity approach for detecting species influenced by mass effect. *J. Appl. Ecol.* **57**, 2031–2040 (2020).

66. S. Dray, R. Pélissier, P. Couteron, M.-J. Fortin, P. Legendre, P. R. Peres-Neto, E. Bellier, R. Bivand, F. G. Blanchet, M. De Cáceres, A.-B. Dufour, E. Heegaard, T. Jombart, F. Munoz, J. Oksanen, J. Thioulouse, H. H. Wagner, Community ecology in the age of multivariate multiscale spatial analysis. *Ecol. Monogr.* **82**, 257–275 (2012).

67. M. J. Anderson, Distance-based tests for homogeneity of multivariate dispersions. *Biometrics* **62**, 245–253 (2006).

68. J. Heino, L. M. Bini, J. García-Girón, F. M. Lansac-Tôha, M. Lindholm, R. J. Rolls, Navigating the spatial and temporal aspects of beta diversity to facilitate understanding biodiversity change. *Glob. Ecol. Conserv.* **56**, e03343 (2024).

69. T. M. Womack, J. S. Crampton, M. J. Hannah, Spatial scaling of beta diversity in the shallow-marine fossil record. *Paleobiology* **47**, 39–53 (2021).

70. D. J. Lunt, A. Farnsworth, C. Loptson, G. L. Foster, P. Markwick, C. L. O'Brien, R. D. Pancost, S. A. Robinson, N. Wrobel, Palaeogeographic controls on climate and proxy interpretation. *Clim. Past* **12**, 1181–1198 (2016).

71. P. J. Valdes, E. Armstrong, M. P. S. Badger, C. D. Bradshaw, F. Bragg, M. Crucifix, T. Davies-Barnard, J. J. Day, A. Farnsworth, C. Gordon, P. O. Hopcroft, A. T. Kennedy, N. S. Lord, D. J. Lunt, A. Marzocchi, L. M. Parry, V. Pope, W. H. G. Roberts, E. J. Stone, G. J. L. Tourte, J. H. T. Williams, The BRIDGE HadCM3 family of climate models: HadCM3@Bristol v1.0. *Geosci. Model Dev.* **10**, 3715–3743 (2017).

71. C. R. Scotese, N. Wright, *PALEOMAP Paleodigital Elevation Models (PaleoDEMS) for the Phanerzoic PALEOMAP Project* (2018). https://www.earthbyte.org/paleodem-resourcescotese-and-wright-2018/.

73. A. Farnsworth, D. J. Lunt, C. L. O'Brien, G. L. Foster, G. N. Inglis, P. Markwick, R. D. Pancost, S. A. Robinson, Climate Sensitivity on Geological Timescales Controlled by Nonlinear Feedbacks and Ocean Circulation. *Geophys. Res. Lett.* **46**, 9880–9889 (2019).

74. S. A. Gagné, R. Proulx, Accurate delineation of biogeographical regions depends on the use of an appropriate distance measure. *J. Biogeogr.* **36**, 561–562 (2009).

75. P. Legendre, L. Legendre, *Numerical Ecology* (Elsevier, 2012).

76. L. Burgener, E. Hyland, E. Griffith, H. Mitášová, L. E. Zanno, T. A. Gates, An extreme climate gradient-induced ecological regionalization in the Upper Cretaceous Western Interior Basin of North America. *GSA Bull.* **133**, 2125–2136 (2021).

77. A. A. Chiarenza, P. D. Mannion, A. Farnsworth, M. T. Carrano, S. Varela, Climatic constraints on the biogeographic history of Mesozoic dinosaurs. *Curr. Biol.* **32**, 570-585.e3 (2022).

78. T. A. Gates, H. Cai, Y. Hu, X. Han, E. Griffith, L. Burgener, E. Hyland, L. E. Zanno, Estimating ancient biogeographic patterns with statistical model discrimination. *Anat. Rec.* **306**, 1880–1895 (2023).

79. R. Amiot, C. Lécuyer, E. Buffetaut, F. Fluteau, S. Legendre, F. Martineau, Latitudinal temperature gradient during the Cretaceous Upper Campanian–Middle Maastrichtian: δ18O record of continental vertebrates. *Earth Planet. Sci. Lett.* **226**, 255–272 (2004).

80. K. G. MacLeod, B. T. Huber, C. Isaza-Londoño, North Atlantic warming during global cooling at the end of the Cretaceous. *Geology* **33**, 437–440 (2005).

81. P. D. Mannion, P. Upchurch, Completeness metrics and the quality of the sauropodomorph fossil record through geological and historical time. *Paleobiology* **36**, 283–302 (2010).

82. C. R. Noto, A. Grossman, Broad-Scale Patterns of Late Jurassic Dinosaur Paleoecology. *PLOS ONE* **5**, e12553 (2010).

83. P. D. Mannion, R. B. J. Benson, P. Upchurch, R. J. Butler, M. T. Carrano, P. M. Barrett, A temperate palaeodiversity peak in Mesozoic dinosaurs and evidence for Late Cretaceous geographical partitioning. *Glob. Ecol. Biogeogr.* **21**, 898–908 (2012).

84. Z. Csiki-Sava, M. Vremir, Ş. Vasile, S. L. Brusatte, G. Dyke, D. Naish, M. A. Norell, R. Totoianu, The East Side Story – The Transylvanian latest Cretaceous continental vertebrate record and its implications for understanding Cretaceous–Paleogene boundary events. *Cretac. Res.* **57**, 662–698 (2016).

85. B. Vila, A. G. Sellés, S. L. Brusatte, Diversity and faunal changes in the latest Cretaceous dinosaur communities of southwestern Europe. *Cretac. Res.* **57**, 552–564 (2016).

86. S. L. Brusatte, C. R. A. Candeiro, F. M. Simbras, The last dinosaurs of Brazil: The Bauru Group and its implications for the end-Cretaceous mass extinction. *An. Acad. Bras. Ciênc.* **89**, 1465–1485 (2017).

87. S. M. Holland, The Stratigraphy of Mass Extinctions and Recoveries. *Annu. Rev. Earth Planet. Sci.* **48**, 75–97 (2020).

88. C. A. Sidor, D. A. Vilhena, K. D. Angielczyk, A. K. Huttenlocker, S. J. Nesbitt, B. R. Peecook, J. S. Steyer, R. M. H. Smith, L. A. Tsuji, Provincialization of terrestrial faunas following the end-Permian mass extinction. *Proc. Natl. Acad. Sci.* **110**, 8129–8133 (2013).

89. Z.-Q. Chen, M. J. Benton, The timing and pattern of biotic recovery following the end-Permian mass extinction. *Nat. Geosci.* **5**, 375–383 (2012).

90. Y. Huang, Z.-Q. Chen, P. D. Roopnarine, M. J. Benton, L. Zhao, X. Feng, Z. Li, The stability and collapse of marine ecosystems during the Permian-Triassic mass extinction. *Curr. Biol.* **33**, 1059-1070.e4 (2023).

91. L. A. Jones, C. D. Dean, W. Gearty, B. J. Allen, rmacrostrat: An R package for accessing and retrieving data from the Macrostrat geological database. *Geosphere* **20**, 1456–1467 (2024).

92. R. F. Butler, E. H. Lindsay, Mineralogy of Magnetic Minerals and Revised Magnetic Polarity Stratigraphy of Continental Sediments, San Juan Basin, New Mexico. *J. Geol.* **93**, 535–554 (1985).

93. E. H. Lindsay, R. F. Butler, N. M. Johnson, Magnetic polarity zonation and biostratigraphy of Late Cretaceous and Paleocene continental deposits, San Juan Basin, New Mexico. *Am. J. Sci.* **281**, 390–435 (1981).

94. D. J. Peppe, D. A. D. Evans, A. V. Smirnov, Magnetostratigraphy of the Ludlow Member of the Fort Union Formation (Lower Paleocene) in the Williston Basin, North Dakota. *Geol. Soc. Am. Bull.* **121**, 65–79 (2009).

95. J. L. Kirschvink, The least-squares line and plane and the analysis of paleomagnetic data. *Geophys. J. Int.* **62**, 699–718 (1980).

96. R. A. Fisher, Dispersion of a sphere. *Proc. R. Soc. A* **217**, 295–305 (1953).

97. G. S. Watson, A test for randomness. *R. Astron. Soc. Geophys. Suppl. Mon. Not.* **4**, 160–161 (1956).

98. P. L. McFadden, M. W. McElhinny, Classification of the reversal test in palaeomagnetism. *Geophys. J. Int.* **103**, 725–729 (1990).

99. W. Lowrie, Identification of ferromagnetic minerals in a rock by coercivity and unblocking temperature properties. *Geophys. Res. Lett.* **17**, 159–162 (1990).

100. A. J. Schaen, B. R. Jicha, K. V. Hodges, P. Vermeesch, M. E. Stelten, C. M. Mercer, D. Phillips, T. A. Rivera, F. Jourdan, E. L. Matchan, S. R. Hemming, L. E. Morgan, S. P. Kelley, W. S. Cassata, M. T. Heizler, P. M. Vasconcelos, J. A. Benowitz, A. A. P. Koppers, D. F. Mark, E. M. Niespolo, C. J. Sprain, W. E. Hames, K. F. Kuiper, B. D. Turrin, P. R. Renne, J. Ross, S. Nomade, H. Guillou, L. E. Webb, B. A. Cohen, A. T. Calvert, N. Joyce, M. Ganerød, J. Wijbrans, O. Ishizuka, H. He, A. Ramirez, J. A. Pfänder, M. Lopez-Martínez, H. Qiu, B. S. Singer, Interpreting and reporting 40Ar/39Ar geochronologic data. *GSA Bull.* **133**, 461–487 (2020).

101. K. F. Kuiper, A. Deino, F. J. Hilgen, W. Krijgsman, P. R. Renne, J. R. Wijbrans, Synchronizing Rock Clocks of Earth History. *Science* **320**, 500–504 (2008).

102. K. Min, R. Mundil, P. R. Renne, K. R. Ludwig, A test for systematic errors in 40Ar/39Ar geochronology through comparison with U/Pb analysis of a 1.1-Ga rhyolite. *Geochim. Cosmochim. Acta* **64**, 73–98 (2000).

562 103. R. H. Steiger, E. Jäger, Subcommission on geochronology: Convention on the use of
563 decay constants in geo- and cosmochronology. *Earth Planet. Sci. Lett.* **36**, 359–362
564 (1977).

565 104. J. R. Taylor, *An Introduction to Error Analysis: The Study of Uncertainties in Physical*
566 *Measurements* (University Science Books, Mill Valley, CA, 1982).

567 105. C. D. Dean, A. A. Chiarenza, S. C. R. Maidment, Formation binning: a new method for
568 increased temporal resolution in regional studies, applied to the Late Cretaceous
569 dinosaur fossil record of North America. *Palaeontology* **63**, 881–901 (2020).

570 106. C. D. Dean, A. A. Chiarenza, J. W. Doser, A. Farnsworth, L. A. Jones, S. J. Lyster, C.
571 L. Outhwaite, P. J. Valdes, R. J. Butler, P. D. Mannion, The structure of the end-
572 Cretaceous dinosaur fossil record in North America. *Curr. Biol.* **35**, 1973-1988.e6
573 (2025).

574 107. R. M. Sullivan, S. G. Lucas, "The Kirtlandian, a new land-vertebrate 'age' for the Late
575 Cretaceous of Western North America" in *Geology of the Zuni Plateau*, S. G. Lucas, S.
576 C. Semken, W. Berglof, D. Ulmer-Scholle, Eds. (New Mexico Geological Society,
577 2003), pp. 369–377.

578 108. P. Legendre, Interpreting the replacement and richness difference components of beta
579 diversity. *Glob. Ecol. Biogeogr.* **23**, 1324–1334 (2014).

580 109. M. Dufrêne, P. Legendre, Species Assemblages and Indicator Species: the Need for a
581 Flexible Asymmetrical Approach. *Ecol. Monogr.* **67**, 345–366 (1997).

582 110. P. D. Mannion, P. Upchurch, M. T. Carrano, P. M. Barrett, Testing the effect of the rock
583 record on diversity: a multidisciplinary approach to elucidating the generic richness of
584 sauropodomorph dinosaurs through time. *Biol. Rev.* **86**, 157–181 (2011).

585 111. M. J. Benton, A. M. Dunhill, G. T. Lloyd, F. G. Marx, Assessing the quality of the fossil
586 record: insights from vertebrates. *Geol. Soc. Lond. Spec. Publ.* **358**, 63–94 (2011).

587 112. N. Brocklehurst, C. F. Kammerer, J. Fröbisch, The early evolution of synapsids, and the
588 influence of sampling on their fossil record. *Paleobiology* **39**, 470–490 (2013).

589 113. J. García-Girón, J. Heino, J. Alahuhta, A. A. Chiarenza, S. L. Brusatte, Palaeontology
590 meets metacommunity ecology: the Maastrichtian dinosaur fossil record of North
591 America as a case study. *Palaeontology* **64**, 335–357 (2021).

592 114. D. Borcard, F. Gillet, P. Legendre, *Numerical Ecology with R* (Springer, New York,
593 NY, 2011; https://link.springer.com/10.1007/978-1-4419-7976-6).

594 115. M. Charrad, N. Ghazzali, V. Boiteau, A. Niknafs, NbClust: An R Package for
595 Determining the Relevant Number of Clusters in a Data Set. *J. Stat. Softw.* **61**, 1–36
596 (2014).

597 116. S. Diem, J. D. Archibald, Range extension of southern chasmosaurine Ceratopsian
598 dinosaurs into northwestern Colorado. *J. Paleontol.* **79**, 251–258 (2005).

599 117. N. Brand, A. Heckert, I. Sanchez, J. Foster, R. Hunt-Foster, J. Eberle, New Upper
600 Cretaceous Microvertebrate Assemblage from the Williams Fork Formation,
601 northwestern Colorado, U.S.A., and its Paleoenvironmental Implications. *Acta*
602 *Palaeontol. Pol.* **67** (2022).

603 118. M. J. Ryan, Evans, "Ornithischian dinosaurs" in *Dinosaur Provincial Park: A*
604 *Spectacular Ancient Ecosystem Revealed*, P. J. Currie, E. B. Koppelhus, Eds. (Indiana
605 University Press, Bloomington, IN, 2005), pp. 312–348.

606 119. F. Fanti, O. Catuneanu, Stratigraphy of the Upper Cretaceous Wapiti Formation, west-
607 central Alberta, Canada. *Can. J. Earth Sci.* **46**, 263–286 (2009).

608 120. F. Fanti, T. Miyashita, A high latitude vertebrate fossil assemblage from the Late
609 Cretaceous of west-central Alberta, Canada: evidence for dinosaur nesting and
610 vertebrate latitudinal gradient. *Palaeogeogr. Palaeoclimatol. Palaeoecol.* **275**, 37–53
611 (2009).

612 121. D. A. Eberth, S. L. Kamo, High-precision U–Pb CA–ID–TIMS dating and
613 chronostratigraphy of the dinosaur-rich Horseshoe Canyon Formation (Upper
614 Cretaceous, Campanian–Maastrichtian), Red Deer River valley, Alberta, Canada. *Can.*
615 *J. Earth Sci.* **57**, 1220–1237 (2019).

616 122. N. R. Longrich, P. J. Currie, *Albertonykus borealis*, a new alvarezsaur (Dinosauria:
617 Theropoda) from the Early Maastrichtian of Alberta, Canada: implications for the
618 systematics and ecology of the Alvarezsauridae. *Cretac. Res.* **30**, 239–252 (2009).

619 123. D. B. Weishampel, J. R. Horner, "Dinosaurs, habitat bottlenecks, and the St. Mary River
620 Formation" in *Fourth Symposium on Mesozoic Terrestrial Ecosystems*, P. M. Currie,
621 E. H. Koster, Eds. (Tyrrell Museum of Paleontology, Drumheller, Alberta, 1987), pp.
622 222–227.

623 124. M. J. Anderson, A new method for non-parametric multivariate analysis of variance.
624 *Austral Ecol.* **26**, 32–46 (2001).

625 125. M. J. Anderson, K. E. Ellingsen, B. H. McArdle, Multivariate dispersion as a measure of
626 beta diversity. *Ecol. Lett.* **9**, 683–693 (2006).

627 126. A. B. Smith, A. J. McGowan, The Shape of the Phanerozoic Marine Palaeodiversity
628 Curve: How Much Can Be Predicted from the Sedimentary Rock Record of Western
629 Europe? *Palaeontology* **50**, 765–774 (2007).

630 127. P. D. Mannion, P. Upchurch, R. B. J. Benson, A. Goswami, The latitudinal biodiversity
631 gradient through deep time. *Trends Ecol. Evol.* **29**, 42–50 (2014).

632 128. M. De Cáceres, P. Legendre, M. Moretti, Improving indicator species analysis by
633 combining groups of sites. *Oikos* **119**, 1674–1684 (2010).

634 129. B. Vilches, M. De Cáceres, D. Sánchez-Mata, R. G. Gavilán, Indicator species of broad-
635 leaved oak forests in the eastern Iberian Peninsula. *Ecol. Indic.* **26**, 44–48 (2013).

636 130. W. Willner, L. Tichý, M. Chytrý, Effects of different fidelity measures and contexts on
637 the determination of diagnostic species. *J. Veg. Sci.* **20**, 130–137 (2009).

131. T. Jombart, S. Devillard, F. Balloux, Discriminant analysis of principal components: a new method for the analysis of genetically structured populations. *BMC Genet.* **11**, 94 (2010).

132. J. A. Thia, Guidelines for standardizing the application of discriminant analysis of principal components to genotype data. *Mol. Ecol. Resour.* **23**, 523–538 (2023).

133. R Core Team, R: A language and environment for statistical computing, R Foundation for Statistical Computing (2023); https://www.R-project.org/.

134. A. A. Chiarenza, A. M. Waterson, D. N. Schmidt, P. J. Valdes, C. Yesson, P. A. Holroyd, M. E. Collinson, A. Farnsworth, D. B. Nicholson, S. Varela, P. M. Barrett, 100 million years of turtle paleoniche dynamics enable the prediction of latitudinal range shifts in a warming world. *Curr. Biol.* **33**, 109-121.e3 (2023).

135. L. A. Jones, K. Eichenseer, Uneven spatial sampling distorts reconstructions of Phanerozoic seawater temperature. *Geology* **50**, 238–242 (2021).

136. P. J. Valdes, E. Armstrong, M. P. S. Badger, C. D. Bradshaw, F. Bragg, M. Crucifix, T. Davies-Barnard, J. J. Day, A. Farnsworth, C. Gordon, P. O. Hopcroft, A. T. Kennedy, N. S. Lord, D. J. Lunt, A. Marzocchi, L. M. Parry, V. Pope, W. H. G. Roberts, E. J. Stone, G. J. L. Tourte, J. H. T. Williams, The BRIDGE HadCM3 family of climate models: HadCM3@Bristol v1.0. *Geosci. Model Dev.* **10**, 3715–3743 (2017).

137. A. Farnsworth, D. J. Lunt, C. L. O'Brien, G. L. Foster, G. N. Inglis, P. Markwick, R. D. Pancost, S. A. Robinson, Climate Sensitivity on Geological Timescales Controlled by Nonlinear Feedbacks and Ocean Circulation. *Geophys. Res. Lett.* **46**, 9880–9889 (2019).

138. A. Farnsworth, D. J. Lunt, S. A. Robinson, P. J. Valdes, W. H. G. Roberts, P. D. Clift, P. Markwick, T. Su, N. Wrobel, F. Bragg, S.-J. Kelland, R. D. Pancost, Past East Asian monsoon evolution controlled by paleogeography, not CO2. *Sci. Adv.* **5**, eaax1697 (2019).

139. N. Sagoo, P. Valdes, R. Flecker, L. J. Gregoire, The Early Eocene equable climate problem: can perturbations of climate model parameters identify possible solutions? *Philos. Trans. R. Soc. Math. Phys. Eng. Sci.* **371**, 20130123 (2013).

140. D. J. Dunlop, Ö. Özdemir, *Rock Magnetism: Fundamentals and Frontiers* (Cambridge University Press, New York, 1997).

141. C. J. Sprain, J. M. Feinberg, P. R. Renne, M. Jackson, Importance of titanohematite in detrital remanent magnetizations of strata spanning the Cretaceous-Paleogene boundary, Hell Creek region, Montana. *Geochem. Geophys. Geosystems* **17**, 660–678 (2016).

142. A. P. Roberts, Magnetic properties of sedimentary greigite (Fe3S4). *Earth Planet. Sci. Lett.* **134**, 227–236 (1995).

143. T. H. Torsvik, R. D. Müller, R. Van der Voo, B. Steinberger, C. Gaina, Global plate motion frames: Toward a unified model. *Rev. Geophys.* **46**, 44 (2008).

144. A. T. Kocsis, N. B. Raja, S. Williams, E. M. Dowding, D. Forschungsgemeinschaft, F. G. Nordbayern, rgplates: R Interface for the GPlates Web Service and Desktop Application, version 0.6.0 (2025); https://cran.r-project.org/web/packages/rgplates/index.html.

145. D. York, Least squares fitting of a straight line with correlated errors. *Earth Planet. Sci. Lett.* **5**, 320–324 (1968).

146. M. D. Cáceres, P. Legendre, Associations between species and groups of sites: indices and statistical inference. *Ecology* **90**, 3566–3574 (2009).

147. A. Kassambara, F. Mundt, factoextra: Extract and Visualize the Results of Multivariate Data Analyses. (2020).

148. J. Oksanen, G. L. Simpson, F. G. Blanchet, R. Kindt, P. Legendre, P. R. Minchin, R. B. O'Hara, P. Solymos, M. H. H. Stevens, E. Szoecs, H. Wagner, M. Barbour, M. Bedward, B. Bolker, D. Borcard, G. Carvalho, M. Chirico, M. D. Caceres, S. Durand, H. B. A. Evangelista, R. FitzJohn, M. Friendly, B. Furneaux, G. Hannigan, M. O. Hill, L. Lahti, D. McGlinn, M.-H. Ouellette, E. R. Cunha, T. Smith, A. Stier, C. J. F. T. Braak, J. Weedon, vegan: Community Ecology Package. *CRAN* (2022).

149. E. Paradis, J. Claude, K. Strimmer, APE: Analyses of Phylogenetics and Evolution in R language. *Bioinformatics* **20**, 289–290 (2004).

Acknowledgements:

This research was supported by the National Science Foundation (EAR 0207750 to TEW and EAR-0207732 [EAR0654096] to AW; EAR 1325544 and DEB 1654952 to TEW and SLB; EAR 1325552 to DJP; and EAR 1325612 to RS), European Research Council (Starting Grant 756226 PalM under the European Union's Horizon 2020 Research and Innovation Programme to SLB; Starting Grant 947921 MAPAS to AAC; Juan de la Cierva-formación 2020 fellowship funded by FJC2020-044836-I/MCIN/AEI/10.13039/501100011033 by the European Union "NextGenerationEU"/PRTR to AAC; Royal Newton International Fellowship NIF\R1\231802 to AAC; Philip Leverhulme Prize to SLB), Geologic Society of America Graduate Research Grant (AGF), Baylor University James Dixon Undergraduate Fieldwork Fellowship (AGF), the European Union Next Generation EU/PRTR (grant no. AG325 for JGG), the British Ecological Society (SR123/1162 for JGG), and the American Chemical Society – Petroleum Research Fund (PRF 52822-DNI8 to DJP). We thank Brittany Abbuhl (Baylor University), Utahna Denetclaw (New Mexico Museum of Natural History and Science), Blake Gorman (Oklahoma State University), Brenton McCullough (Oklahoma State University), Jonathan Meserve (Tufts University), and Krister Smith (University of California) for fieldwork assistance and the Bureau of Land Management for providing collecting permits and supporting our research.

Author contributions

A.G.F., S.L.B., A.A.C., J.G-G., R.S., M.T.H., T.E.W., and D.J.P designed the study. A.G.F., S.L.B., A.J.D., R.S., S.S., A.W., T.E.W., and D.J.P. collected paleomagnetic samples and measured lithostratigraphic sections used in this study. A.G.F., A.J.D., C.W.F IV, C.E.L., and D.J.P. analyzed and interpreted paleomagnetic samples. A.G.F. and D.J.P. conducted rock magnetism analyses. M.T.H. and New Mexico Geochronology Research Laboratory staff

separated sanidine grains for detrital ages, whereas M.T.H. performed all analyses, and calculated $^{40}Ar/^{39}Ar$ ages. S.L.B., A.A.C., J. G-G., and T.E.W. updated Late Cretaceous-Paleocene vertebrate occurrence information and performed all provinciality analyses.

Competing interests

The authors declare no competing interests.

Data Availability

All data that support the findings of this study, including raw paleomagnetic data, are included as supplementary files and are uploaded to the Texas Data Repository (https://dataverse.tdl.org/privateurl.xhtml?token=6544d576-d3fa-4e90-a340-e43a9a75afa1) for permanent archiving prior to publication.

List of Supplementary Materials:

Materials and Methods
Figs. S1 to S12
Tables S1 to S32

Fig. 1:

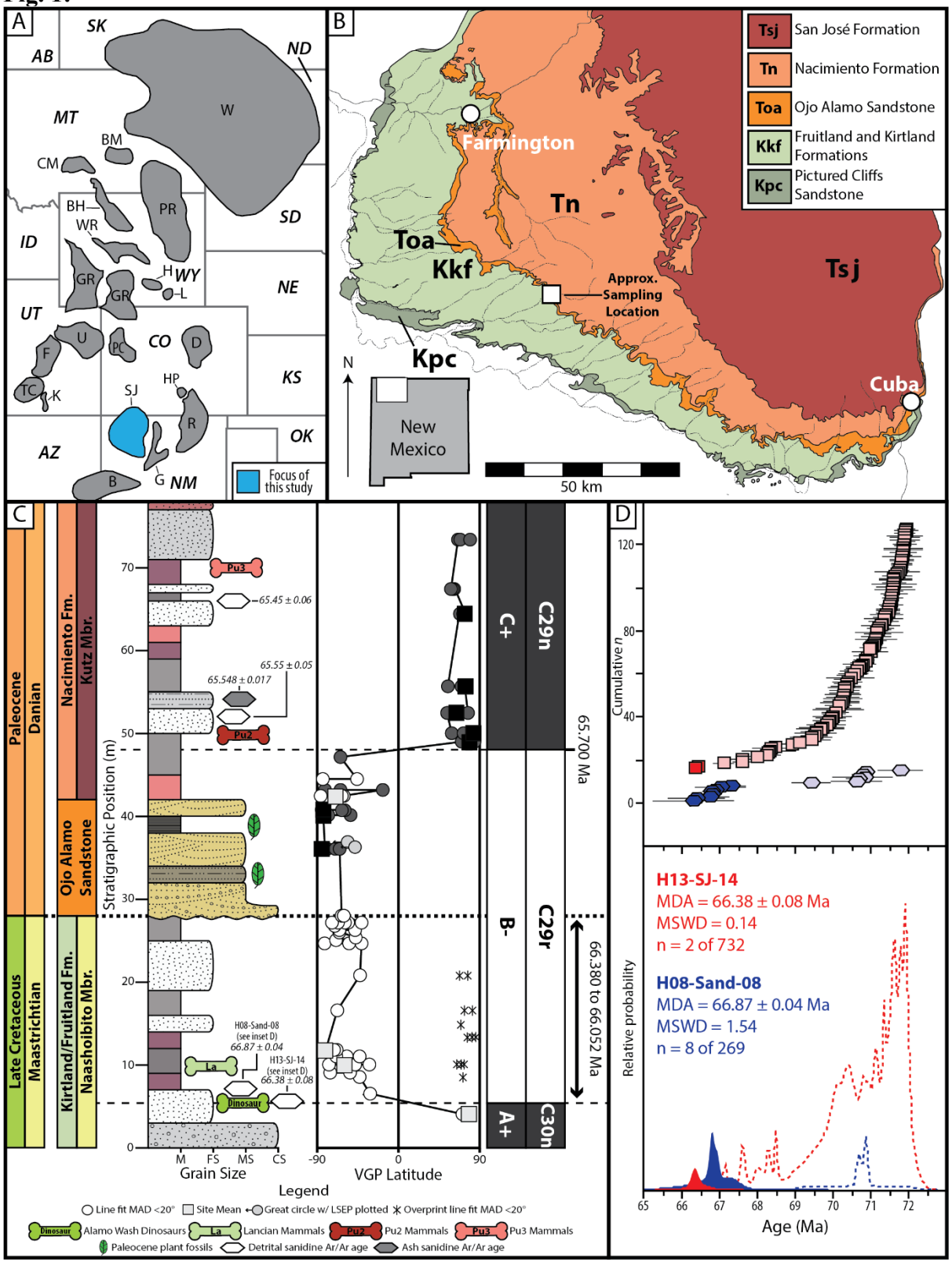

Fig. 1. Latest Cretaceous to early Paleocene San Juan Basin chronology (**A**) regional map of western North America showing major late Cretaceous and early Paleogene terrestrial depositional basins: B - Baca, BH – Bighorn, BM – Bull Mountain, CM – Crazy Mountain, D – Denver, F – Flagstaff, G – Galisteo, GR – Green River, H – Hanna, HP – Huerfano Peak, K – Kaiparowits, L – Laramie, PC – Piceance Creek, PR – Powder River, R – Ration, SJ – San

Juan, TC – Table Cliffs, U – Uinta, W – Williston, WR – Wind River. (**B**) Geologic map of the San Juan Basin showing major lithologic units and sampling location for this study (modified from *39*). (**C**) Composite measured section showing major lithologic units, stratigraphic position of vertebrate and plant fossil horizons and sanidine age dates, virtual geomagnetic pole (VGP) latitude (white fill – this study; grey fill – (*40*)) and interpreted local polarity zonation correlated with the GPTS. Grain sizes: M- mud, FS – fine sand, MS – medium sand, CS – coarse sand. (**D**) Detrital sanidine age data from samples H13-SJ-14 and H08-Sand-08. The solid fill age probability distribution is the data defining the MDA, whereas the dashed line is the full distribution of the data shown in the upper panel.

Fig. 2:

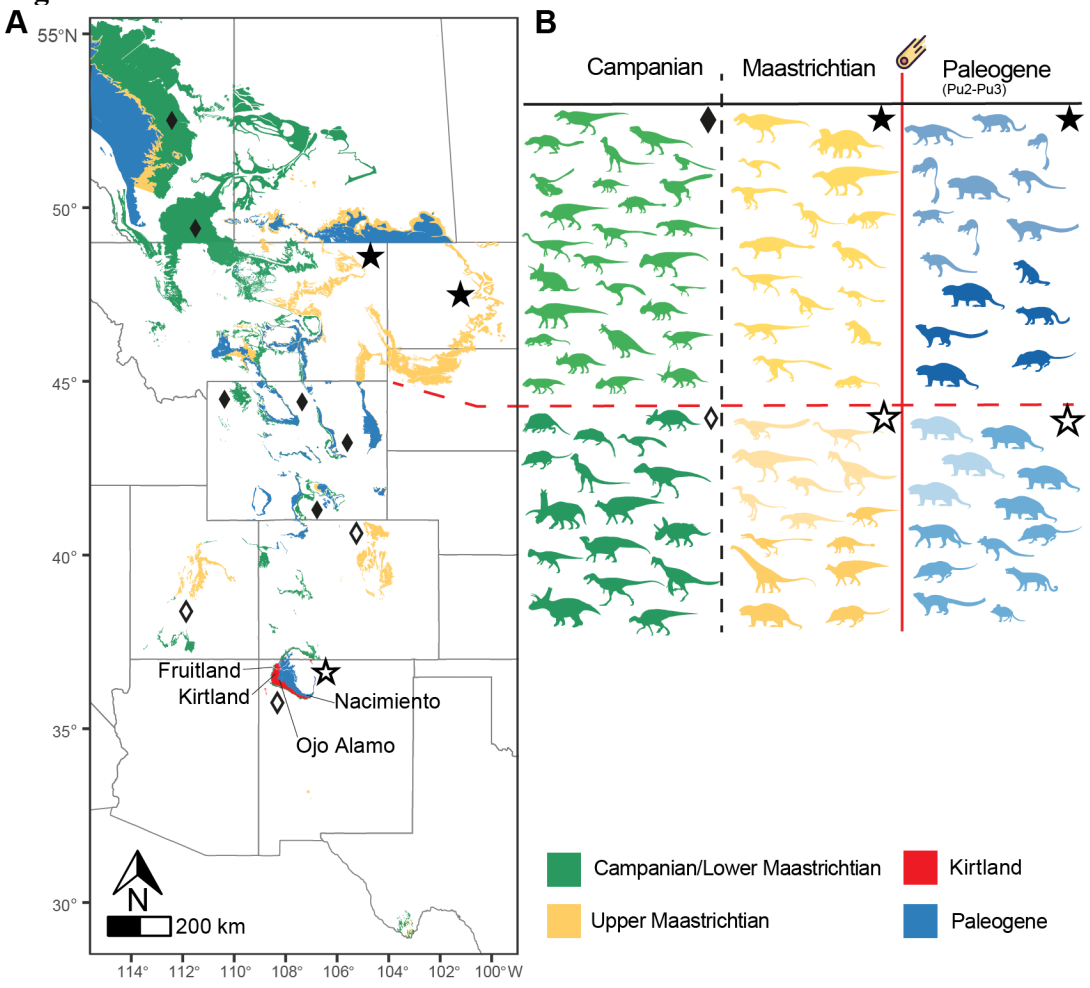

Fig. 2. Latest Cretaceous-early Paleogene terrestrial basins in western North America and their faunas. (**A**) Judithian (Campanian–Lower Maastrichtian) localities in green, Upper Maastrichtian in yellow, early Paleocene in blue. Diamonds mark Campanian sites (black = north, white = south); stars highlight Hell Creek and San Juan Basin. Red in Kirtland Fm. denotes the Naashoibito Mbr., focus of this study. **(B)** Silhouettes of vertebrates from this interval: darker = southern endemics, lighter = cosmopolitan taxa.

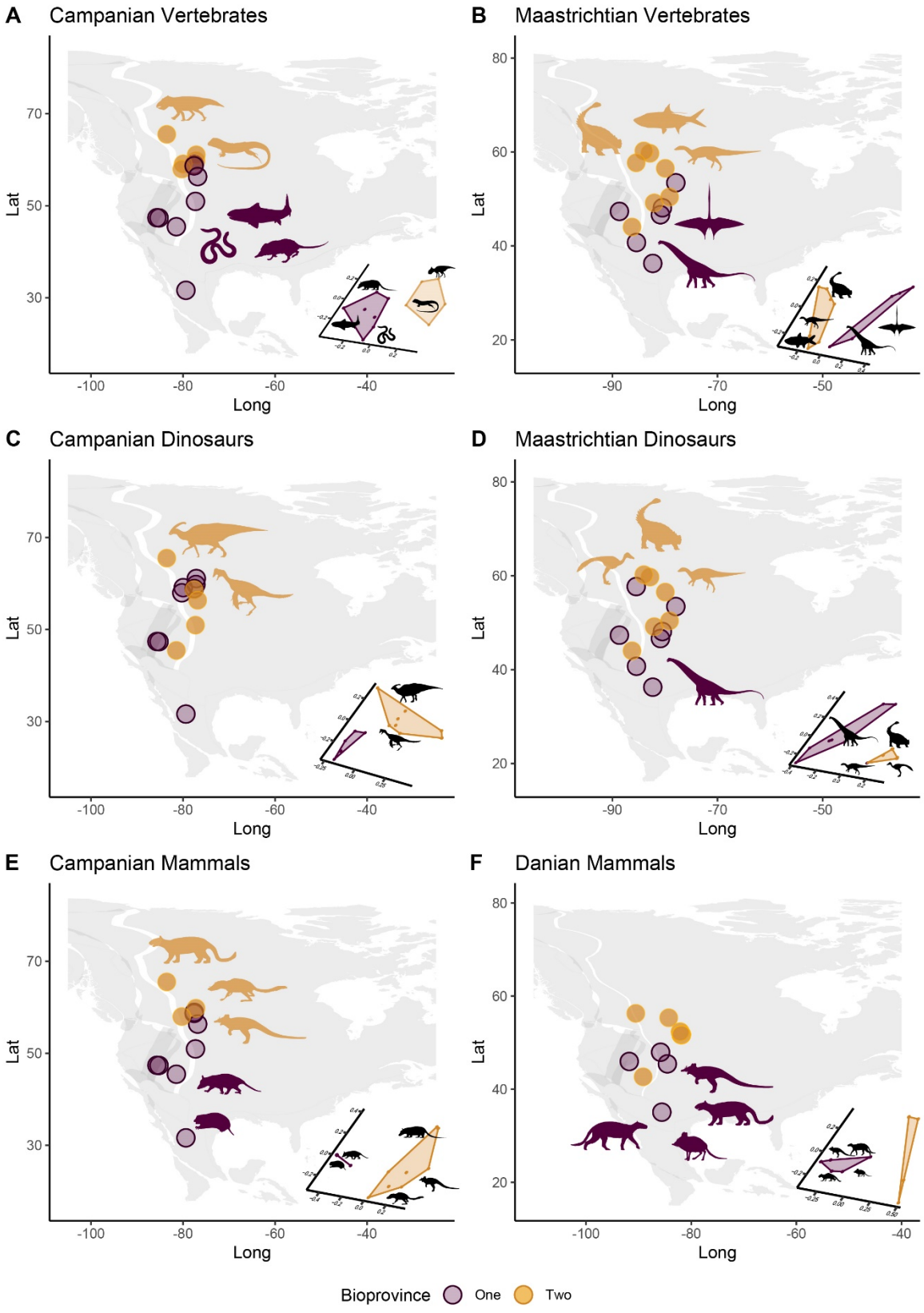

Fig. 3. Latest Cretaceous–early Paleogene vertebrate bioprovinces across North America with representative taxa. Hypothesized faunal provinces (as defined in Table S12); silhouettes representative of animals associated to each bioprovince following Table S24. Ordination plots from Figure S8, where the identification of silhouettes are also identified.

Supplementary Materials for:

Late-surviving New Mexican Dinosaurs illuminate high end-Cretaceous diversity and provinciality

Andrew G. Flynn, Stephen L. Brusatte, Alfio Alessandro Chiarenza, Jorge García-Girón, Adam J. Davis, C. Will Fenley IV, Caitlin E. Leslie, Ross Secord, Sarah Shelley, Anne Weil, Matthew T. Heizler, Thomas E. Williamson, Daniel J. Peppe

Corresponding authors: agflynn@nmsu.edu, matt.heizler@nmt.edu, thomas.williamson@dca.nm.gov, daniel_peppe@baylor.edu

Supplemental Figures and Tables:

Figure S12 – Relative contributions of different paleoenvironmental variables to faunal provinciality

MATERIALS AND METHODS

Lithostratigraphy

Lithostratigraphic sections were measured through the Naashoibito Member of the Fruitland Formation and the Ojo Alamo Sandstone in the Bist/De-Na-Zin Wilderness area from five locations (magnetostratigraphy measured section names in parathenses) – (1) Barnum Brown Amphitheater (P11NB), (2) Hunter Wash (P13HW), (3) mammal site L4005 in Alamo Wash (L4005), (4) Log Jam Locality (P14LJ), and 5) the "34-Bone" Site of Hunt and Lucas (1991) (Fig. S1). Lithostratigraphic sections were measured at all locations where paleomagnetic samples were collected. All sections were measured to the nearest decimeter using a Jacob's staff and an Abney hand level (Fig. S1). The lithology, grain size, stratigraphic thickness, sedimentary structures, and any biological features (i.e., roots, fossil leaves, and vertebrate fossils) were documented for each stratigraphic unit. Lithostratigraphic units of the Western Interior Basin were plotted in Figure 2 using the R package rmacrostrat (*91*)

Magnetostratigraphy

Paleomagnetic samples were collected in the Bisti/De-Na-Zin Wilderness area from four stratigraphic sections in the Naashoibito Member (sections: Log Jam Locality, Hunter Wash, L4005 mammal site, and Barnum Brown Amphitheater) (Figure 1; Table S1) by D. Peppe, A. Flynn, A. Davis, and T. Williamson. The Barnum Brown Amphitheater section was also sampled, at a lower sampling resolution by (*56, 92*, *93*). The Barnum Brown Amphitheater section was collected through the entire thickness of the Naashoibito Member. The Log Jam Locality section was measured and sampled through the top of the Naashoibito, the complete thickness of the Ojo Alamo Sandstone, and the base of the Nacimiento. Two sections were collected through a partial section of the Naashoibito Member, one at Alamo Wash (section: L4005) and another at nearby Hunter Wash (section: Hunter Wash) (Fig. 1).

Oriented paleomagnetic block samples were collected from 27 sampling horizons spanning the Naashoibito Member of the Kirkland Formation (n = 23), Ojo Alamo Sandstone (n = 2), and lowermost Kutz Member of the Nacimiento Formation (n = 2) at approximately 2.5 m intervals (minimum: 0.25 m; maximum: 9.25 m). At each sampling horizon, a trench was dug to remove any weathered material and four separately oriented block samples were collected. A flat face was shaved on the *in situ* sample using a hand rasp and the strike and dip of that face was measured using a Brunton pocket transit compass. Samples were collected from a range of lithologies and grain sizes from mudstone to fine grained sandstone. At Baylor University, the block samples were dry cut into ~1 cm^3 cubes using a lapidary saw.

Samples were measured at Baylor University using an automated three-axis DC-SQUID magnetometer housed inside a two-layer magnetostatic shield with a background field typically less than 300 nT. The samples were demagnetized using a combined alternating-field (AF) and thermal demagnetization strategy following the methods of (*94*). All samples were first given a low-AF (2.5-10.0 mT in 2.5 mT increments) pre-treatment using a 3-axis automated static alternating field device to remove and low-coercivity viscous or isothermal remanence. Ten to fifteen thermal demagnetization steps were then performed from 75-100 °C to the maximum unblocking temperature (typically 250-400 °C) in a controlled nitrogen atmosphere to minimize

oxidation reactions. Progressive thermal demagnetization was carried out until the magnetic intensity of the samples fell below noise level or the measured directions became erratic and unstable.

The characteristic remanence for samples with quasi-linear trajectories was isolated using principal-component analyses (PCA) (*95*). Best-fit lines were calculated when a minimum of three demagnetization steps that has a maximum angle of deviation (MAD) less than 20° and trended toward the origin (Table S5). Samples that were analyzed by great circles were used if the MAD was less than 20° (Table S7). Samples with an erratic demagnetization behavior were excluded from analyses. Site mean directions were calculated from sampling localities with 3 reliable line-fit samples with an $\alpha_{95} \leq 35°$ (Table S6) (*96*). Sites with an alpha 95 (α_{95}) value greater than 35°, which exceeds the cut-off value based on the randomness criteria of (*97*), were excluded. All raw paleomagnetic data is archived at the Texas Data Repository: https://dataverse.tdl.org/privateurl.xhtml?token=6544d576-d3fa-4e90-a340-e43a9a75afa1

Reversal boundaries were placed at the stratigraphic midpoint between samples of opposing polarities. The stratigraphic position of each reversal was calculated relative to the Ojo Alamo-Nacimiento formational contact. The resulting local polarity stratigraphy was then correlated to the Geomagnetic Polarity Time Scale (GPTS) (*57*). The data presented in this paper was correlated with Flynn et al., 2020 to estimate the total thickness of C29r.

Many specimens' demagnetization trajectories turned toward the origin after a few steps and were fully demagnetized by 200 to 400 °C (Figure S1). Eighty-one samples from 27 sampling horizons were analyzed as part of this study. Reliable paleomagnetic directions using best-fit lines were generated for 40 samples (49.4%) from 19 sampling horizons (70.4%) (Fig. S2A; Table S5). Great circles were calculated from 3 samples (3.7%) from 3 sampling horizons (11.1%) (Table S7). Four of the sampling horizons (14.8%) passed our site-mean selection criteria (i.e., three or more samples that could be used to calculate a site mean with an $\alpha95 < 35°$). The mean normal and reversed directions calculated using Fisher (1953) statistics are also shown. The mean normal declination and inclination for lines are 355.6° and 43.1° (n = 3, a95 = 21.1°) and for sites are 355.6° and 43.1° (n = 1). The reversed declination and inclination for lines are 180.4° and -47.4° (n = 37, a95 = 9.0°) and for sites is 186.9° and -51.8° (n = 3, a95 = 17.5°). The dual polarity mean direction (i.e., all declinations and inclinations converted to normal polarity) for lines is 359.9° and 47.1° (n = 40, a95 = 8.3°) and for site is 003.5° and 50.1° (n = 4, a95 = 19.5°). Using the mean normal and reversed directions for lines, the reversed and normal groups do not share a common distribution with >95% confidence, but the hypothesis that they share a common mean at >95% confidence cannot be rejected (i.e., negative reversals test) (*98*). This result is likely due to the very small sample size of normal directions. Due to the small number of samples, it was not possible to conduct a reversals test on the site mean directions. Using the dual-polarity mean direction, we calculated a paleomagnetic pole from the Naashoibito, Ojo Alamo, and Nacimiento from 40 line-fit samples and 4 site means at 84.0 °N and 065.5 ° (*n* = 40, K = 6.5, A95 = 9.6°) and 77.8 °N and 003.1° (*n* = 4, K = 2.7, A95 = 70.1°), respectively.

As expanded on in the Rock Magnetism section, we identified a portion of normal polarity from ~10-20 m (Fig. 1C) that we interpreted to represent overprinted directions and not the characteristic remanent direction. This is an interval that previously was correlated with a normal polarity chron (*58*). We interpret this interval as normal polarity because 1) this normal interval is underlain by our detrital Ar/Ar date of 66.38 ± 0.08 Ma and the only Cretaceous magnetic polarity chron younger than 66.38 Ma is C29r, 2) this overprinted interval is bounded

on both sides by significant line-fit and site mean reversed polarity samples, and 3) of the 6 sampling horizons with significant normal polarity overprint, three horizons also produce significant line-fit reversed polarity directions. Taken together, we interpret this entire interval as indicating a part of our section with diagenetic overprint and these normal polarity directions are not Cretaceous directions.

Rock magnetism

Triaxial isothermal remanent magnetization (IRM) Lowrie Test (*99*) was performed on 4 samples from the Naashoibito Member at Baylor University to determine the primary and secondary magnetic carriers in mixed mineralogy samples. Samples from variable lithologies were chosen to represent the range of magnetic mineralogies present in the Naashoibito Member. A 1 T, 300 mT, and 100 mT was imparted along the X, Y, and Z axes, respectively, of paleomagnetic block samples using an ASC pulse magnetizer. Samples were then thermally demagnetized in 25 °C increments from 100-200 °C and 50 °C from 200-700 °C using an ASC N_2 atmosphere. The magnetization in the X, Y, and Z axes was measured at each temperature step using a 2G cryogenic DC-SQuID magnetometer. All rock magnetism raw data is archived at the Texas Data Repository: https://dataverse.tdl.org/privateurl.xhtml?token=6544d576-d3fa-4e90-a340-e43a9a75afa1.

Ar/Ar Geochronology

The analytical data are organized to comply with FAIR data reporting norms (*100*). Multiple Excel workbooks are provided with data formatted in a variety of manners to facilitate ease of data viewing (Tables S7-S11). Data are presented in isotope ratio format along with raw intensity format with the raw data sorted by run identifier and sample name.

Sandstone samples were crushed and sieved to between 40 and 120 mesh, washed in tap water and exposed to dilute HCl in an ultrasonic bath. The samples were thoroughly rinsed in distilled water and dried before concentrating K-feldspar with heavy liquid density separation. While being viewed under a binocular microscope, the clear K-feldspar grains were handpicked to concentrate detrital sanidine (DS) from microcline and orthoclase. Grains that yielded Precambrian ages are very likely not sanidine, while grains less than ca. 300 Ma are very likely sanidine.

Samples were irradiated in four packages at either the USGS reactor in Denver, Colorado or the Oregon State reactor. Irradiations were NM-248 (85 hours), NM-254 (40 hours), NM-265 (32 hours), and NM-335 (21 hours). DS crystals were placed in holes drilled around the perimeter of 1” diameter aluminum trays. All irradiations included FC-2 Fish Canyon sanidine interlaboratory standard in a known geometry to determine neutron flux. In all cases, FC-2 was loaded in the same trays as the unknowns and there are 6 to 20 flux monitor locations within the trays. Typically 6 or 8 individual grains from each monitor hole are analyzed and the J-value of the unknown locations is determined with a planar fit to the appropriate flux monitor locations. FC-2 is assigned an age of 28.201 Ma (*101*) and all ages are calculated with a ^{40}K decay constant of 5.463e-10 /a (*102*) while isotope abundances are after (*103*).

After irradiation, monitors and unknowns were loaded into copper or stainless steel trays, evacuated and baked at temperatures between 100 and 150°C for 1 to 4 hours. The single crystals were fuse or step-heated with a CO_2 laser. Crystals are typically heated for 30 seconds, followed by 30 seconds of gas cleanup using a cold D50 and NP-10 getter and a hot NP-10 getter. Isotopes were analyzed using a ThermoFisher Scientific ARGUS VI multi-collector mass spectrometer

(system Jan) equipped with five Faraday cups, and one electron multiplier (CDD) operated in ion-counting mode. The configuration has ^{40}Ar, ^{39}Ar, ^{38}Ar, ^{37}Ar and ^{36}Ar on the H1, Axial, L1, L2, and CDD detectors, respectively. Resistors were either 10^{12} or 10^{13} Ohms for ^{40}Ar and ^{39}Ar and either 10^{12} or $10^{14}$for ^{38}Ar and ^{37}Ar. ^{36}Ar was measured on the CDD that has a dead time of 14 ns.

Calibration gases of air and a gas mixture enriched in radiogenic ^{40}Ar along with ^{39}Ar were analyzed interspersed with the unknowns to monitor instrument drift and determine detector intercalibration factors. Data collection was conducted with either MassSpec version 7.875 (NM-248, NM-254) or in-house Pychron software (NM-265, NM-335) and all data reduction utilized MassSpec version 7.875. Isotopes were collected for 120 to 400 seconds followed by 35 to 180 seconds of baseline measurement. Analyses were truncated based on various criteria to facilitate efficient data collection. For instance, relatively old grains that did not contribute significantly to MDA determination or provenance were analyzed for shorter durations than the late Cretaceous grains.

Extraction line blank behavior was relatively constant throughout this study owing to overall similar analytical protocols. Following sample tray bakeout, ^{40}Ar and associated atmospheric ^{36}Ar were elevated and decreased throughout the course of data collection that typically took about 1-2 days to complete a sample run of 221 crystals. Blank (including mass spectrometer backgrounds) are given for each analysis in the raw intensity worksheets. Because of generally low blanks and backgrounds relative to signal size, calculated ages are not sensitive to these corrections for the unknowns and standards. K-glass and CaF_2 were included in the irradiations to determine interfering reaction correction factors.

The reported MDA's are derived from combination of the youngest normally distributed total fusion dates and integrated dates. Both the MDA and plateau ages derived from step-heated grains are calculated based on a weighted mean with a weighting factor being the inverse variance (e.g., *104*) and the error is the square root of the sum of $1/\sigma^2$ values. The error is also multiplied by the square root of the MSWD for MSWD greater than 1 and errors are reported at 1σ. J-error and irradiation correction factor uncertainties are included for all weighted mean age errors.

The detrital sanidine age data are summarized in Figure S7 and Table S13. The age spectra for step-heated crystals generally record flat or nearly flat age patterns; demonstrating simple argon systematics with no detectable problems associated with post-deposition argon loss. Single crystals of sample H08-Sand-08 was investigated extensively using high precision incremental heating (Table S7, Figure S5). Because the grains used for determining the MDA of H08-Sand-08 are flat, their plateau ages are nearly identical to integrated ages and thus integrated ages are combined with total fusion ages to obtain the grand total of dates used to define the MDA. That is, the age probability plot of this sample combined step-heated derived integrated dates with total fusion dates. Sample SJ-SS-Bone is from the same locality as H08-SJ-08 and had a generally older distribution of ages, likely related to it being coarser-grained and that nearly clear microcline and orthoclase grains were chosen instead of sanidine grains. Sample H13-SJ-14 was dated in two separate irradiations and all data are combined to yield the MDA. For the second irradiation (NM-335) improved detrital sanidine picking methods resulted in many more dates less than 75 Ma compared to the first irradiation of this sample. The two youngest total fusion ages yield the preferred MDA.

Faunal provinciality

Vertebrate occurrence data

We used an updated version of the dataset of (*16*) (Tables S26-S31) for all terrestrial and fluvio-lacustrine vertebrates from the Campanian–Danian of Laramidia, in which the ages of the latest Cretaceous taxa followed the new geochronological results presented here. We built this dataset from records in the Paleobiology Database (PBDB: https://paleobiodb.org/), which we scrutinized for accuracy based on our team's expertise on the anatomy and classification of vertebrate fossils. We assigned taxonomic categories based on the least inclusive clade to which we could contribute each fossil. This mostly coincided with "family-level" clades (e.g. Adocidae, Ankylosauridae, Baenidae). When less-inclusive clades could be recognized, with different taxa from the same "family-level" clade co-occurring, sub-familiar taxonomic ranks were used (e.g. Chasmosaurinae vs Centrosaurinae, Saurolophinae vs Lambeosaurinae, Velociraptorinae vs Saurornitholestinae). When fossils could not be assigned confidently to a less inclusive category (often the case with small and rare terrestrial fossils), broader, supra-specific clades were used instead (e.g., Pycnodontiformes, Scincomorpha, Pediomyoidea). The fossil dataset includes more than 470 taxa represented by ca. 1,600 occurrences of dinosaurs (including birds), mammals, crocodylians, champsosaurs, turtles, squamates, albanerpetontids, salamanders, frogs, and cartilaginous and bony fish. We present our full dataset, with detailed references for individual taxa and ages of faunas, in Tables S26-S31. Although we carefully vetted the original PBDB records when initially building the dataset, we realize that large community-constructed open-access databases may have occasional incorrect or inconsistent records. For this reason, as detailed below, we performed a series of bootstrapping sensitivity analyses demonstrating the robustness of our results when records for individual taxa and localities are iteratively removed and resampled (Figs. S9-S11).

Statistical modeling

We used our dataset to test whether there was faunal provinciality during the Campanian, Maastrichtian, and Danian. To do so, we tested for the optimal number of bioprovinces in each of the three time intervals, and then explored whether the bioprovinces changed over time, and which environmental and geographic factors were most important in underpinning them. In choosing to do our primary analyses using age-level time bins, we follow the rationale of recent studies of latest Cretaceous faunal evolution (*16*), as the age-level provides a trade-off between age resolution and sample size (ever-smaller time bins would result in ever-smaller sample sizes per bin, compromising statistical power, and introducing potential errors as many of the faunas cannot be accurately dated to a sub million-year resolution).

However, although our primary analyses utilize age-level bins, we conducted sensitivity analyses at a finer temporal resolution in order to test the robustness of our results. This is also to address previous studies on the terminal Cretaceous record of North America that have highlighted high volatility in detected diversity patterns at decreasing final resolution (*105, 106*). We repeated the analyses at the finest temporal resolution we could resolve in our dataset, which is at the level of North American Land Mammal Ages, or NALMAs. These sensitivity analyses binned taxa into Judithian (late Campanian-early Maastrichtian), Lancian (late Maastrichtian), and Danian (early Paleocene) bins. We were not able to include an Edmontonian (early-mid Maastrichtian) bin because of insufficient sample size (only two faunas could be reliably assigned to this age), which limited the statistical power necessary for reliable inference. Included within our Judithian bin are faunas that some authors assign to another short biozone, the Kirtlandian, which comes at the very end of the traditional Judithian (*42, 107*) We find that it

is challenging in practice to confidently distinguish between Judithian and Kirtlandian faunas, given that direct radioisotopic dates are limited for these faunas, and the Kirtlandian (if valid) is very short. Resolution of finer time slices within NALMAs is not currently possible for our dataset, as most sub-NALMA bins would have too few faunas to provide robust statistical signal, and because the age uncertainty of many faunas would span sub-NALMA bin boundaries, necessitating the fauna to be assigned to multiple sub-NALMA bins, compromising detection of a genuine signal of change over time.

For our primary analyses and all sensitivity tests, we first displayed the Hellinger-transformed presence-absence fossil occurrence matrices using principal coordinate analysis (PCO) computed on the square root of the Jaccard dissimilarities to avoid negative eigenvalues (*108*). We then obtained the residual 'unexplained' signals from the resulting orthogonal PCO axes (*109*) using the number of discrete vertebrate-bearing collections as a proxy for the unequal distribution of sampling effort (*110–112*) following the step-by-step approach in (*16*, *113*). *K*-means partitioning based on residual eigenvectors was run to identify high-density regions in the data (*114*) and cluster Laramidian assemblages for each time interval (Campanian–Danian) based on the similarity of their constituent taxa, the optimal number of bioprovinces being estimated with the sum of squared distances (*115*).

As a sensitivity analysis, we further generated 100 bootstrap occurrence matrices through a random resampling of the original dataset comprising fossil-bearing localities and associated vertebrate taxa. This sensitivity analysis allowed an explicit assessment of the consistency and robustness of the inferred bioprovince delineations to some issues that can affect a large-scale data compilation such as ours: i) sampling bias in taxonomic occurrences (taxa might have been unreported or missing from our dataset, either because they have yet to be collected by paleontologists or because they have been collected but were missed when compiling the records of the PBDB); ii) taxonomic opinions which may vary and affect the alpha-diversity of a locality or assemblage (expert opinions may differ on cases of taxon synonymy, lumping vs. splitting classification strategies, and assignment of fragmentary remains to higher-level taxa, all affecting the taxonomic assignment of records in the PBDB); iii) inaccuracies in the dating of faunas (not all localities are directly dated by radioisotopic techniques, radioisotopic dates can change with new data, and some faunas are close to time bin boundaries and could conceivably span them). Specifically, we quantified the congruence of bioprovince assignments for each locality across all bootstrap replicates by calculating the frequency of consistent assignments (Figs. S9-S11).

We also performed a series of sensitivity analyses which addressed the issue of some faunas crossing age boundaries (Tables S14-S15, S18-S19. S22-S23). When designing these analyses, we followed this rationale:

Other than an age-level division (Campanian, Maastrichtian and Danian), the chronology of the dataset follows the formation-level binning procedure of (*105*). The revised file assigns each occurrence to one of four chronostratigraphic bins that strike a balance between temporal resolution and adequate sample size: the North American faunal stages Judithian, Edmontonian, and Lancian, plus the Danian. In this framework the Judithian bin now explicitly encompasses the Lower Kaiparowits, middle–upper Wahweap, Fruitland, Aguja, Dinosaur Park, Foremost, Judith River, Oldman and Two Medicine formations. The Mesaverde Group, represented by the Williams Fork Formation, remains in the Edmontonian bin because its fossiliferous horizons lie almost entirely within the upper Campanian and its internal dating is not robust enough to resolve sub-stage divisions (*116, 117*) likewise, Kaiparowits data have been retained in the Judithian bin (*35*). All of these choices were verified against the most recent radiometric and

magnetostratigraphic compilations used elsewhere in the manuscript (*35, 118-120*). Because most well-dated Horseshoe Canyon Formation vertebrates fall between 72.2 and 72.6 Ma (firmly Campanian according to (*121*)) and because our Maastrichtian focus is chiefly on the Lancian, we treat the HCF as Campanian during stage-level analyses; taxa from demonstrably later horizons, for example the Maastrichtian *Albertonykus* (from the upper, Unit 4 of the HCF; (*121, 122*) were already separated in the spreadsheet to the early Maastrichtian, and that practice is now stated explicitly. A similar rationale governs our handling of "Mesaverde" data, which we equate with the Williams Fork Formation: the microvertebrate localities that supply virtually all records lie within Campanian strata, so the entire Williams Fork is retained in the Campanian unless new evidence of key Maastrichtian taxa can be documented. The St. Mary River Formation presents a different problem because its placement varies in the literature: Fowler (2017) assigns nearly all of it to the Maastrichtian, whereas earlier sources (e.g., *123*) regard the lower part as late Campanian or earliest Maastrichtian. Given our emphasis on Lancian assemblages, the revised dataset excludes the St. Mary River from the Lancian data altogether and assigns its occurrences to an early-Maastrichtian (Edmontonian) bin.

Finally, we considered the suggestion of binning at member level. After trial runs, we concluded that the requisite census data are too sparse and unevenly sampled for most formations, and that such fine-scale subdivision would introduce more noise than temporal precision. Similarly, because our Edmontonian time bin on its own contained only two faunas, we had to exclude it from analyses because it did not have the statistical power to deliver meaningful results for testing whether there was one or more bioprovince.

Once the number of bioprovinces for each time interval was determined, we performed a permutational multivariate analysis of variance (PERMANOVA) (*124*) with 999 permutations to test for mean differences in assemblage composition among these hypothesized faunal provinces. This permutation-based *F*-test may indicate differences in (i) across-bioprovince dissimilarities in terms of assemblage composition, (ii) within-bioprovince dispersion, or (iii) both (*124*). Hence, to test the null hypothesis that there was no difference in the internal variation of the bioprovinces for each time interval, we ran a test of homogeneity of multivariate dispersion (PERMDISP) (*66*, *125*) with 999 permutations of least-squares residuals. Because the levels of the grouping factor introduced as arguments for these resemblance-based permutation analyses and subsequent statistical routines (below) were those obtained from residual eigenvectors, our model estimates cannot be attributed to the confounding effect of sampling biases (e.g., *126*, *127*).

Indicator species analysis (sensu *109*) was conducted to identify target taxa that were statistically significant indicators of different faunal provinces (*128*). These associations were tested for statistical significance using 999 permutations and we retained only those taxa with an indicator value index (IndVal) greater than 0.5 (*129*), which denoted target species characterizing individual bioprovinces in our case (*130*). Please note that an indicator species does not equate to the presence of an 'index taxon' *unique* to a specific bioprovince, but rather a collection of taxa that are statistically *associated* (i.e. their co-occurrence) to a specific bioprovince (i.e. without implying that any single or multiple taxa are exclusively confined to a specific bioprovince).

To further understand the mechanistic nature of the bioprovinces, we applied discriminant analysis of principal components (DAPC) (*131*), a popular approach for the analysis of spatially structured populations (*134*). This identifies paleoenvironmental gradients (i.e., elevation, *m*; paleolatitude, º; paleolongitude, º; near-surface (1.5 m) mean annual temperature, *ºC*; near-surface (1.5 m) annual temperature SD, *ºC*; annual average precipitation, *mm*; annual

precipitation SD, *mm*; and net primary productivity, *g C* m^{-2} $year^{-1}$) that maximized discrete biogeographical separation among the hypothesized bioprovinces (*132*).

DAPC is a versatile multivariate routine applicable to any quantitative data—such as paleoecological data and fossil records. Here, we combined principal component analysis and discriminant analysis to summarize large-scale biological dissimilarities among different faunal provinces determined by *k*-means partitioning. In other words, we used DAPC to infer individual contributions of different paleoenvironmental variables to the existence of cross-continental discrete bioprovinces in terrestrial and fluvio-lacustrine vertebrates across the K–Pg boundary. All statistical analyses were run in the R environment v. 4.3.0 (*133*), and the detailed list of packages and routines are available from Table S21.

Paleoenvironmental data

Paleoclimatic and land-surface model outputs come from the HadCM3BL-M2-1aE version of the fully coupled atmosphere-ocean GCM HadCM3L v. 4.5 model (*71*), whereas paleogeographies are those from the grid-based paleo-digital elevation model (DEM) (*72*). Simulations and settings (e.g. orbital configuration, spin-up procedure, initial and boundary conditions) for all Late Cretaceous and early Paleogene paleoenvironmental models are described in full by (*70–72*). Details on deep-time general circulation models and additional information of their experimental design and paleontological applications can also be found in (*14–16*, *77*, *134*).

We here expand on our decision to utilize our chosen paleoenvironmental modelling approach, rather than climate and environmental proxies from specific Late Cretaceous formations that include the terrestrial fossils in our dataset.

Proxy data are inherently spatially uneven, with certain formations and regions more densely sampled than others. This spatial heterogeneity introduces significant sampling biases and limits the applicability of such data for regional-to-continental scale quantitative analyses, particularly when correlating proxies with broad distributional patterns of species (i.e. macroecological patterns). This limitation has been explicitly demonstrated in recent work (e.g., *135*), which showed that uneven spatial sampling can distort macroecological and paleoclimatic reconstructions. Because many formations span large geographic areas and temporal ranges, it is difficult to assign a single local proxy-derived MAT or plant assemblage to represent entire formation-level climatic conditions. Climate model outputs, on the other hand, provide continuous, spatially explicit climate surfaces (e.g., MAT, MAP, cold/warm month means), allowing us to assign consistent environmental data across the full extent of a formation or locality, reducing interpretative ambiguity and enhancing comparability. While proxies offer more direct evidence of past conditions, they are often subject to complex diagenetic histories, differential preservation, and interpretative uncertainties (e.g. mixed floral assemblages, taphonomic biases, or variation in isotopic signals due to non-climatic factors). These limitations can introduce noise in comparative ecological analyses like DAPC, especially when integrating across multiple formations and regions.

The HadCM3L-M2.1D and HadAM3B-N216 paleoclimate models we used are well-established and extensively validated in both modern and paleoclimate frameworks (e.g., *136-138*). These models incorporate realistic reconstructions of topography, ocean circulation, dynamic vegetation, and atmospheric chemistry (e.g. pCO_2), and are fully equilibrated over more than 9,000 model years to ensure climatological stability. Notably, HadCM3-based models have shown good agreement with proxy data, including high-latitude temperature reconstructions

under various climate states (e.g., *139*). Finally, the HadCM3 models include the TRIFFID dynamic vegetation module, which allows for climate–vegetation feedbacks. While the plant functional types used are necessarily based on modern analogues (due to the lack of detailed Mesozoic equivalents), this approach still captures broad climate–vegetation interactions relevant to macroecological patterns. Proxy plant provinces, by contrast, are more difficult to quantitatively incorporate into a DAPC framework without introducing subjective interpretation.

Given these reasons, we hold that spatially explicit paleoclimate model outputs provide a more suitable framework for testing regional ecological differentiation (e.g. bioprovinciality) than sparse and often localized proxy data.

EXPANDED RESULTS

Summary of geochronology results

Ar/Ar Geochronology

We conducted detrital sanidine $^{40}Ar/^{39}Ar$ geochronology on two dinosaur bone-bearing Naashoibito localities, where 1046 total grains were dated from three individual samples (Tables S8-S11). Both single crystal laser fusion and step-heating experiments were conducted (Tables S7 – S11). There is a wide range of Cretaceous and Mesozoic total fusion and integrated ages with 491 crystals yielding dates less than 75 Ma (Fig. 1D). Samples H08-Sand-08 and SJ-SS-bone were collected from a sandstone channel ~20.0 m below the Naashoibito-Ojo Alamo contact and ~5 m above the basal conglomerates of the Naashoibito (Fig. 1C). H08-Sand-08 yields a maximum depositional age (MDA) of 66.87 ± 0.04 Ma derived from a normal distribution (mean squared weight deviation (MSWD) = 1.54) of eight dates (Fig. 1D). Importantly, seven of these eight dates are integrated ages derived from step-heating analyses that yield flat single crystal age spectra demonstrating that the dated crystals have not experienced argon loss (Tables S7-S8). Sample SJ-SS-Bone from this same site did not yield grains less than 70 Ma and gives an MDA of 72.61 ± 0.21 Ma based on the nine youngest grains. This sample was coarser grained than H08-Sand-08 and yielded many old grains (>300 Ma) that are like orthoclase and microcline. Sample H13-SJ-14 is directly from the dinosaur-bearing "34-Bone Site", a medium-grained sandstone approximately 3.5 m above the base of the Naashoibito Member (*56*), which contains the partial skeleton of a lambeosaurine hadrosaur. All detrital sanidines (N = 732) from this sample are total fusion dates and 24 dates are less than 70 Ma (Tables S7-S11) with the youngest two grains yielding an MDA of 66.38 ± 0.08 Ma (Fig 1D). Thus, we have identified two dinosaur fossil-bearing samples that are significantly younger than 70 Ma (i.e., that previous suggested age for the Naashoibito from Jasinski et al., 2011), with H13-SJ-13 (from the 34-Bone Site) isotopically dated to be less than 400 Kyr from the K-Pg boundary.

Magnetostratigraphy

The magnetostratigraphic analyses from this study identified two local polarity zones within our section: 1) A+ at the base of the Naashoibito Member and 2) B- which incorporates the upper Naashoibito Member, entire Ojo Alamo Sandstone, and basal Nacimiento Formation (Fig. 1C, Table S2). The MDAs of the isotopically dated samples H13-SJ-14 (66.38 ± 0.08 Ma) and H08-Sand-08 (66.87 ± 0.04 Ma) constrain local polarity zones A+ and B- to magnetochrons C30n and C29r of the Geomagnetic Polarity Timescale (GPTS) (cf., *57*), respectively. Magnetochrons C30n and C29r are the only Cretaceous normal and reversed polarity subchrons

younger than 66.87 Ma (Fig. 1C-D) (*57*) and the interpreted reversal boundary directly underlies our youngest MDA of 66.38 ± 0.08 Ma. This magnetostratigraphic interpretation is further supported by a sanidine date from an ash overlying the Nacimiento Formation of 65.548 ± 0.017 Ma (*40*), which indicates the reversed polarity chron that incorporates the Naashoibito Member, Ojo Alamo Sandstone, and basal Nacimiento Formation can only be C29r (Fig. 1C). The age of the C30n-C29r reversal (66.380 Ma) (*57*) further supports our isotopic MDAs for the Naashoibito and constrains the MDA of the upper ~22 m of the Naashoibito Member, including major dinosaur-bearing horizons, to within 340 Kyr before the K-Pg boundary (Fig. 1C) indicating the Naashoibito fauna is latest Maastrichtian in age and contemporaneous with the Hell Creek faunas from the Northern Great Plains. The Naashoibito fauna is separated from the earliest Paleocene Nacimiento fauna, which lacks mammals of early Puercan (Pu1 biozone) age, by ~700 Kyr (Fig. 1C-D).

Lastly, we identified an interval of normal polarity in the Upper Cretaceous (from approximately 10-20 m) that previous work had erroneously correlated with a normal polarity zone of the GPTS (*58*). Our new analyses indicate this is an interval of significant diagenetic overprint of the paleomagnetic signal within a zone of reversed Cretaceous polarity (see next section for fill discussion on magnetic overprint; Fig. S4).

The Naashoibito dinosaur fauna is diverse and includes a variety of species: dromaeosaurid, oviraptorosaurian, ornithomimid, troodontid, and tyrannosaurid theropods; titanosaurian sauropods; and ankylosaurian, ceratopsid, and hadrosaurid ornithischians (*48*). It does not appear abnormal or depauperate compared to earlier faunas (*16*), and its diversity levels never did not garnered attention previously when the Naashoibito fauna was thought to be four million years older (*42*). Therefore, it appears that dinosaurs were apparently thriving in New Mexico within the few hundred thousand years before the asteroid impact, and probably until the very end of the Cretaceous, with no obvious signs of any local decline.

The coeval nature of the Naashoibito and Hell Creek faunas gives new improved insight into regional similarities and differences in vertebrate faunas before the end-Cretaceous extinction. The northern Hell Creek fauna appears more diverse than the southern Naashoibito fauna during the latest Cretaceous, but the former is much better sampled (*14,* Supplementary Data). However, these two faunas share few species-level taxa and major dinosaur groups present in the more poorly sampled south (e.g., the titanosaurian sauropod *Alamosaurus*, lambeosaurine hadrosaurs) are absent in the north, despite over a century of intense collecting. These differences extend to mammals, as the multituberculate *Essonodon* and metatherian *Glasbius* are common in the San Juan BasinNaashoibito, but very rare in the Hell Creek. However, the apex predator *Tyrannosaurus* is present in both faunas (*48*), indicating that it, by comparison to some of the other less cosmopolitan faunal elements of each of these latest Maastrichtian biological provinces, ranged widely across western North America.

However, these comparisons are qualitative, as have been most discussions thus far on Late Cretaceous dinosaur biogeography and faunal evolution. This necessitates our faunal provinciality analyses, below.

Rock magnetism

The triaxial IRM Lowrie tests for all samples indicate a mixed mineralogy of samples in the Naashoibito. The majority of samples include grains with coercivities from 100 – 300 mT and retain remanence above 400 °C until they are fully demagnetized between 550–600 °C, which indicates the presence of (titano)magnetite (Fig. S4) (*140*). In a subset of samples, there is

a large drop in remanence between 100-200 °C in the low coercivity fraction (grain less than 100 mT) (Figure S4A, 4D) indicating intermediate titanohematite (*141*). In another subset of samples, the Triaxial IRM Lowrie Fuller tests indicates the occurrence of maghemite and/or hematite due to the high proportion of remanence held in the >1 T coercivity, the abrupt loss of remanence at >650 °C, and the red or purple coloring of the sample (Figs. S4B, S4C) (*141*). Finally, in some samples, we interpret the presence of greigite, which converts to (titano)magnetite above 400 °C, based on the large drop in the 0-300 mT coercivities between 200 and 300 °C (Fig. S4B) (*142*).

The demagnetization behavior of samples from the Naashoibito exhibited three primary types of behavior: (1) samples with erratic demagnetization behavior, (2) samples that record an overprint direction, and (3) samples that record the primary Cretaceous direction. Generally, samples that behaved erratically were unstable from very low temperatures and were often fully demagnetized by temperatures ≤300 °C (Fig. S2D). We interpret these samples to have a relatively high proportion of titanohematite, which is easily reset and frequently overprinted (*140*, *141*). Samples that recorded an overprint direction were generally stable to temperatures >400 °C and were red or purple in color. The triaxial IRM Lowrie test indicated grains with coercivities >1T (Fig. S4B and S4C). We interpret these samples to be dominated by diagenetic hematite or maghemite that record a post-depositional overprint direction. These results are similar to previous rock magnetic analyses of the Naashoibito (e.g., *92*) who documented the occurrence of samples with a high coercivity (>300 mT) and a high maximum unblocking temperature (>320 °C using non-controlled atmosphere thermal demagnetization), which they interpreted to be hematite created by post-depositional oxidation. Samples that documented a primary Cretaceous direction were typically stable to 300 – 400 °C, and triaxial IRM Lowrie tests indicate the presence of (titano)magnetite and other minerals (titanohematite, hematite/maghemite, greigite) (Fig. S2D-F, Fig. S4). We interpret this to mean that (titano)magnetite was the primary magnetic carrier and samples with a relatively high proportion of (titano)magnetite produced reliable magnetic directions, while samples with a small proportion of (titano)magnetite and a high proportion of titanohematite or hematite produced erratic or overprint directions.

Summary of faunal provinciality results

We applied multivariate and resemblance-based methods from metacommunity ecology and biogeography (e.g., *63–66*) to assess whether there was faunal provinciality during the latest Cretaceous (Campanian and Maastrichtian) and earliest Paleocene (Danian), and if so, what underpinned it. Our analyses utilized an inclusive dataset of terrestrial and fluvio-lacustrine vertebrates, unlike many previous studies that focused only on dinosaurs (e.g., *26–30*). We conducted our analyses at the age-level (Campanian, Maastrichtian, Danian), in line with other recent studies (e.g., *30*, *31*), because sub age-level analyses with these methods are not currently feasible, given the quality of the fossil record and age uncertainties of some fossil-bearing formations.

We tested for the optimal number of bioprovinces in time interval, using the sum of squared distance method on *k*-means partitioning. This identified two optimal bioprovinces (k = 2) for all three intervals (Table S12) and faunal stages (Table S13) after accounting for potential biases in the fossil record when all terrestrial and fluvio-lacustrine vertebrates were considered (Fig. S8). These hypothesized faunal provinces were robust to sensitivity analyses at increased chronostratigraphic resolution after applying formation binning methods (Tables S14-S15).

Moreover, the robustness of these patterns also remained after bootstrap resampling of taxa and fossil localities (Figs. S9-S11), which provides further strength to our interpretations. Overall, these findings suggest that there was large-scale faunal provinciality during the Campanian and Maastrichtian that was maintained across the K–Pg boundary into the Danian (Figs. 2 and 3).

We assessed the structure of these bioprovinces over time. We found that the provinces were significantly different in assemblage composition in the Late Cretaceous and early Paleogene (Figs. 2 and 3, Tables S16-S19), although they did not differ in their amount of internal variation in the lead-up to, or after, the extinction event (Table S20-S23). In other words, bioprovinces across the K–Pg boundary differed in terms of their mean assemblage composition, but not in their spatial beta diversity (i.e., the spatial variability in community composition between two or more localities with a spatial region of interest) (*67–69*). Different taxa (Fig. 2) statistically characterized the different provinces over time (Table S24 and S25). For instance, the association (e.g., co-occurrence) of a few dinosaurian lineages (Leptoceratopsidae, Albertosaurinae, Microraptoria), teiid lizards, and bony fish (Gonorynchiformes, Osteoglossomorpha) were indicators of northernmost faunal provinces during the Campanian and Judithian faunal stage, whereas the association of several lineages of squamates (Anguimorpha), ray-finned fishes (Lepisosteiformes), and freshwater turtles (Compsemydidae, Trionychidae) were indicators of the relatively more southern bioprovinces in the Danian (see Tables S26-S31). Please note that this does not imply these taxa are exclusive to either hypothesized biozone, but rather that their associations within each biozone are statistically significant in distinguishing one biozone from the other.

Finally, we explored the environmental and geographic factors most responsible for the bioprovinces, with discriminant analysis of principal components (DAPC) on a dataset including information on elevation, latitude, longitude, temperature, precipitation (both including mean annual and seasonality values), and other ecogeographical factors from Cretaceous–Paleocene paleoenvironmental models (*70–73*). Our results provide compelling evidence that vertebrate provinciality across the K–Pg boundary was partially controlled by temperature, with spatial location also having a role in the first few million years after the extinction (Fig. S12). Thus, thermal constraints were most instrumental in explaining the bioprovinces, not strictly north-south geographic separation, although geography did play a secondary role.

We performed two subsidiary analyses, in which we applied our methods to datasets containing only dinosaurs and only mammals (Fig. 3C-F). For dinosaurs, we also obtained two optimal bioprovinces for both the Campanian and Maastrichtian, with slightly different boundaries than those in our all-vertebrate dataset (Fig. 3A-B; Table S12). Differences in assemblage composition among bioprovinces were readily apparent both at the age-level (Table S16) and across different faunal stages (Table S17). For instance, the association of lambeosaurine hadrosaurs and caenagnathid oviraptorosaurs were among the major indicator species during the Campanian. These taxa were further associated with leptoceratopsids and microraptorians in the bioprovince containing the Dinosaur Provincial Park region (Fig. 3C-D; Table S24). Some ornithischians (Ankylosauridae, Thescelosauridae) and small-sized theropods (Troodontidae) contributed significantly to the split between bioprovinces in the terminal Cretaceous, and the giant sauropod *Alamosaurus* was mostly restricted to the southern boundaries of the Western Interior during the Maastrichtian (Tables S24 and S25). The DAPC analysis indicates temperature as a driver of dinosaur provinciality during the final few million years of the Cretaceous (Fig. S12).

Mammals were divided into two bioprovinces during the Campanian (Fig. 3E), then exhibited increased cosmopolitanism in the Maastrichtian (partitioning clustering identified no discrete subgroups or clusters, although sample size was probably not adequate to test for number of bioprovinces; Tables S12 and S13), followed by an increase in biogeographical separation after the mass extinction (Fig. 3F; Fig. S8; Table S12). Rather than a strict north-south divide, discrete bioprovinces were also somewhat separated in the early Paleogene along an east-west gradient (Fig. S12), with different eutherian lineages (e.g. the mouse-sized leptictids and macroscelidians, and the sheep-to-cow-sized pantodonts and phenacodontids) generally associated with the well-sampled sequences from the northern Great Plains and the fossil-rich southern Nacimiento Formation (Table S24).

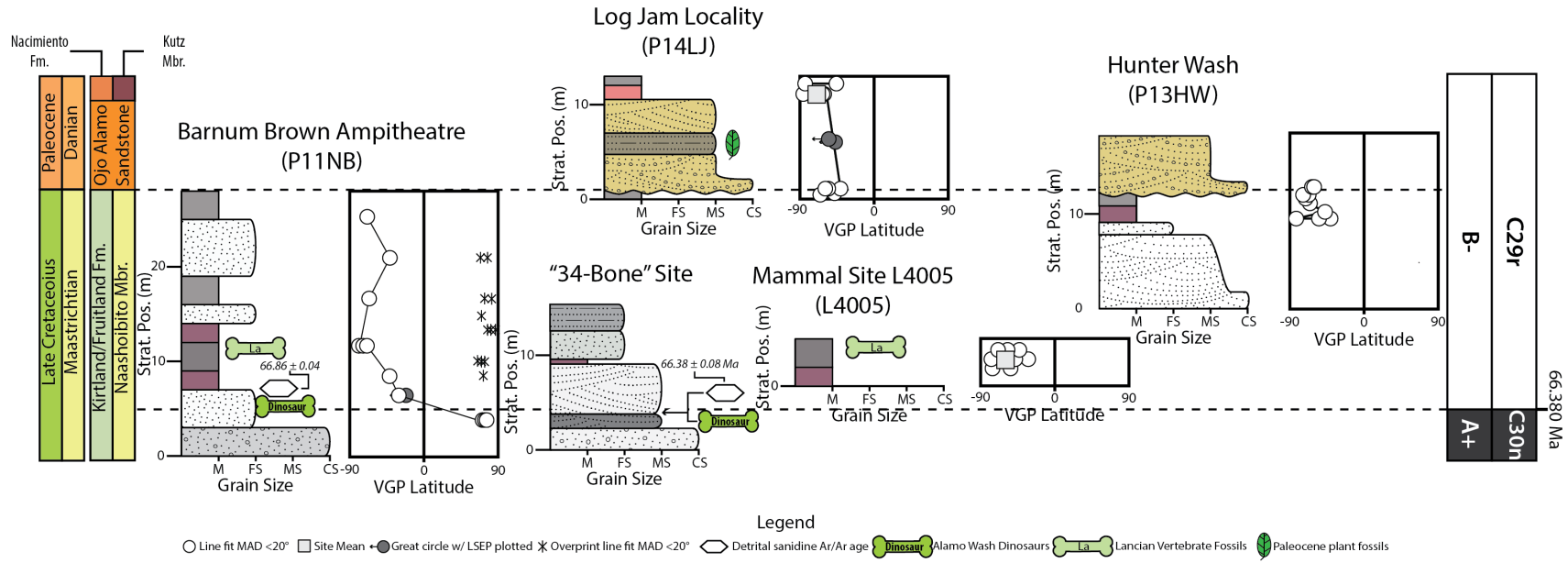

Fig. S1. Correlation of the five litho- and magnetostratigraphic sections used in this study – (1) Barnum Brown Amphitheatre (P11NB), (2) Mammal Locality L4005 (L4005), (3) Log Jam Locality (P14LJ), (4) Hunter Wash (P13HW), and (5) "34-Bone" Site – showing the major lithologic units, virtual geomagnetic pole (VGP) latitude, local polarity stratigraphy, and correlation with the GPTS. The lithologic contact between the Naashoibito Member and Ojo Alamo Sandstone was used as a datum. Grain sizes are located at the bottom of each section: M – mud, FS – fine sand, MS – medium sand, CS – coarse sand. Stratigraphic position of vertebrate fossil horizon and detrital sanidine MDAs shown.

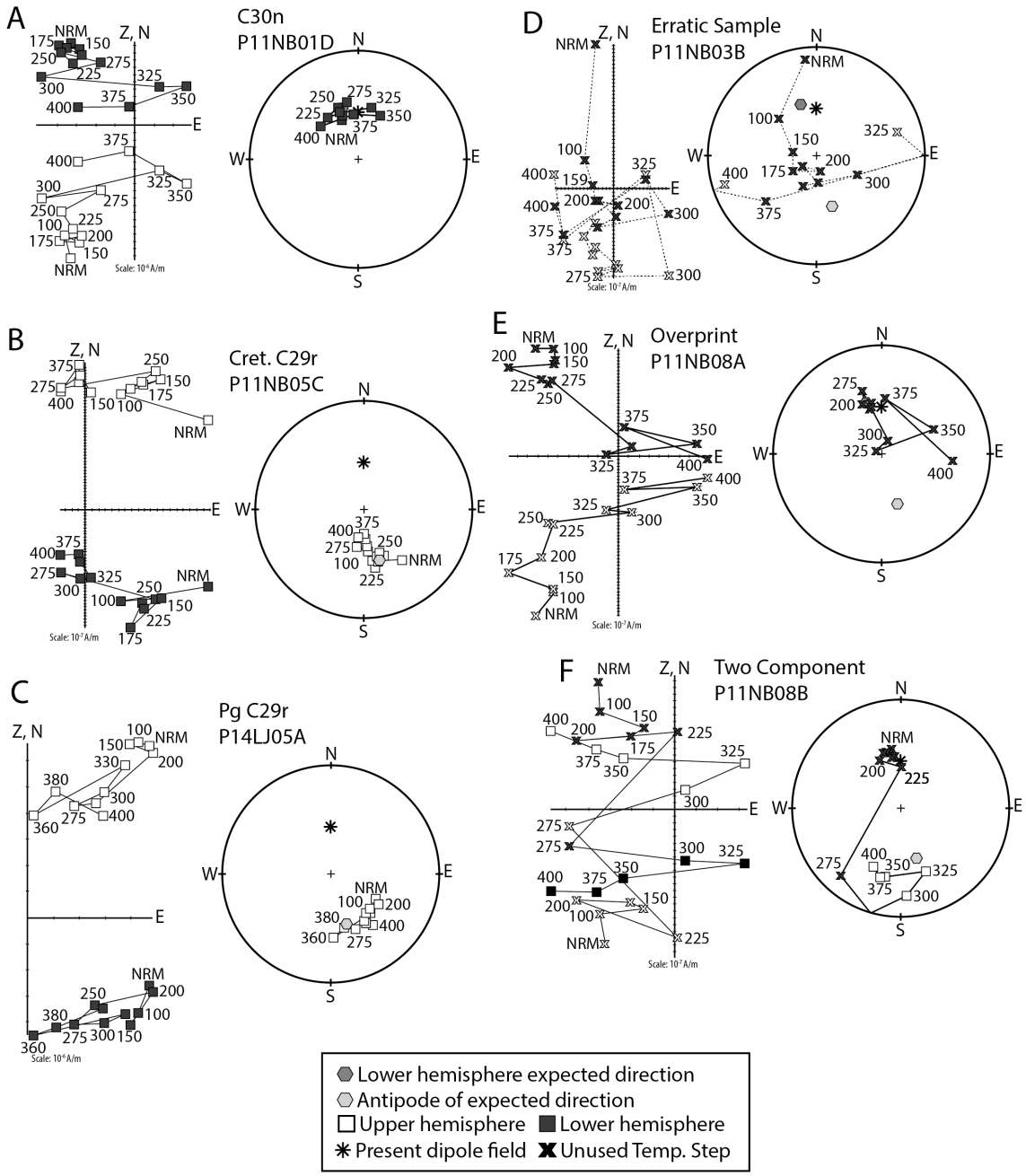

Fig. S2. Representative orthogonal end vector demagnetization diagrams for each subset of paleomagnetic data (A-C). Demagnetization trajectories for C30n (A), Cretaceous C29r (B), and Paleogene C29r (C) samples which allowed for line fitting to determine a characteristic direction. (D) Representative sample where line fitting was not possible due to the erratic nature of the data and was not used in any interpretation. (E-F) Samples for sampling horizon P11NB08 which show an interpreted overprint direction sample due to stable normal direction until unblocking temperature and becoming erratic and a two component sample where step heating has removed the overprint diagenetic mineralogy (~275-300 °C) allowing for line-fitting reversed direction.

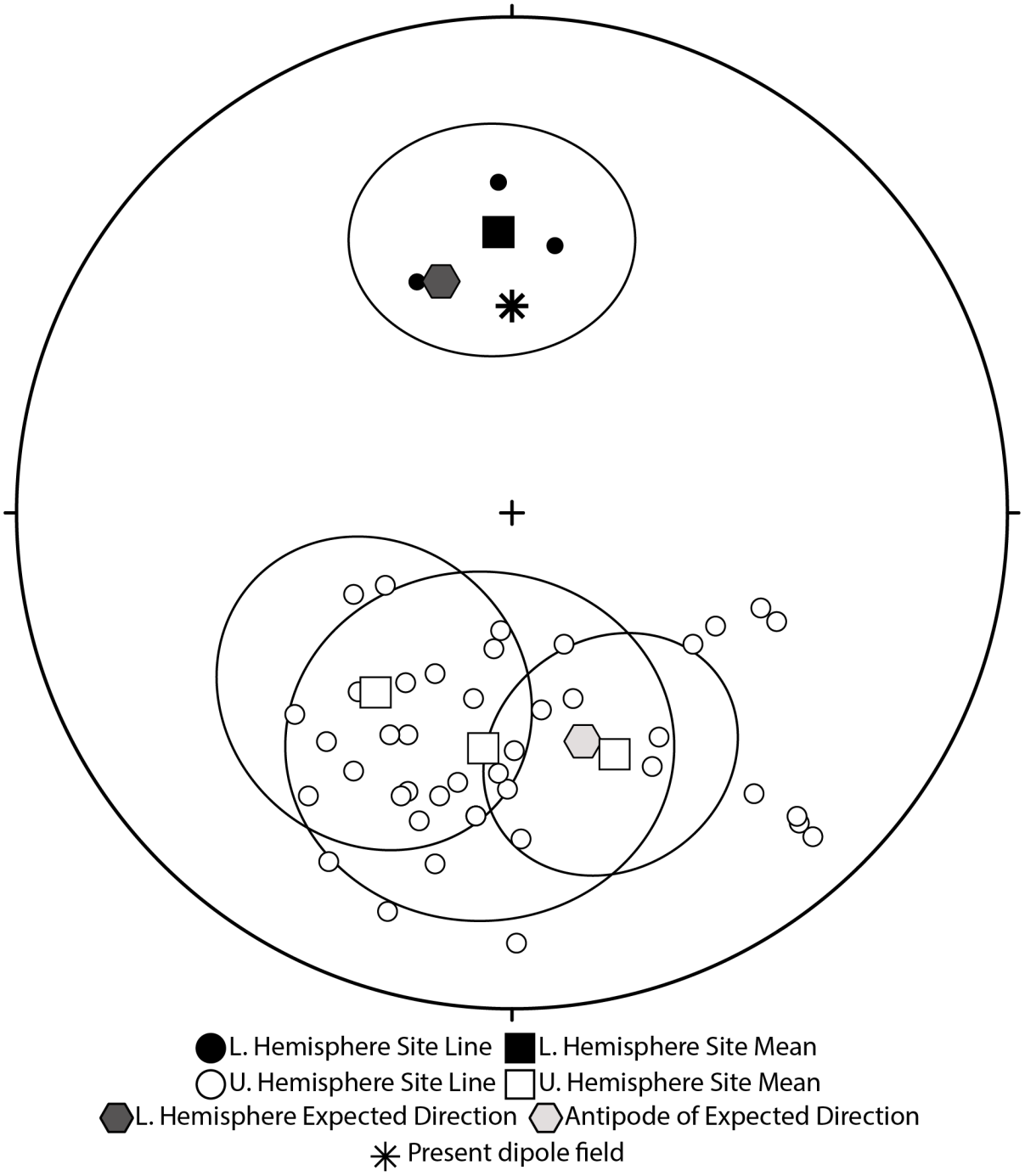

Fig. S3. Equal area plot showing all line-fitted characteristic magnetization directions (Table S4) and all site-mean directions calculated (Table S5) calculated for this study. The modern dipole, expected latest Cretaceous direction recalculated from (*143*), and the antipode of the expected latest Cretaceous direction are shown. Ellipses indicate errors on site mean estimates.

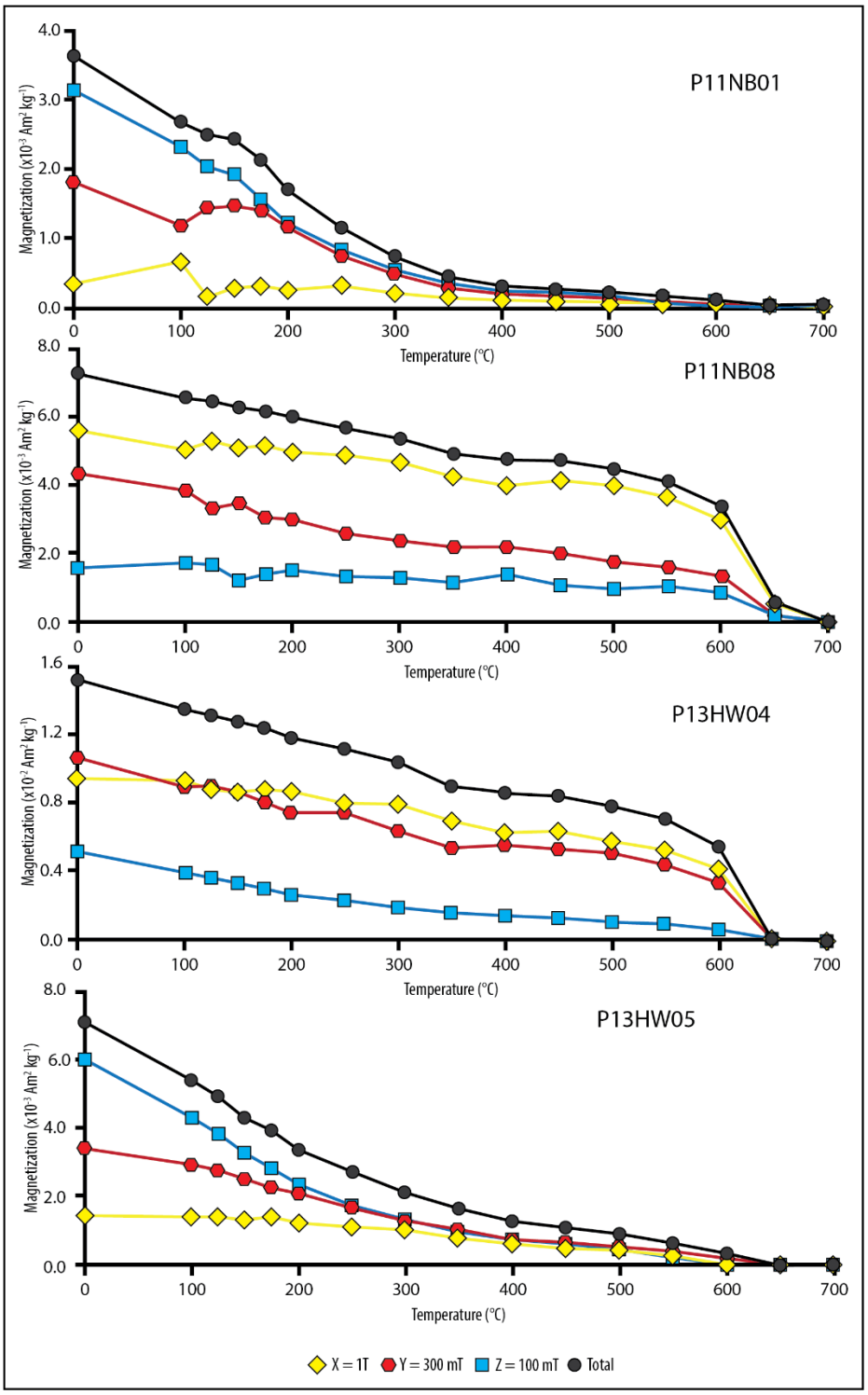

Fig. S4. Thermal demagnetization curves of orthogonal isothermal remanent magnetization (IRM) imparted along the X, Y, and Z axes for four samples from the Naashoibito member following the methods of (*99*). See supplement text for full discussion.

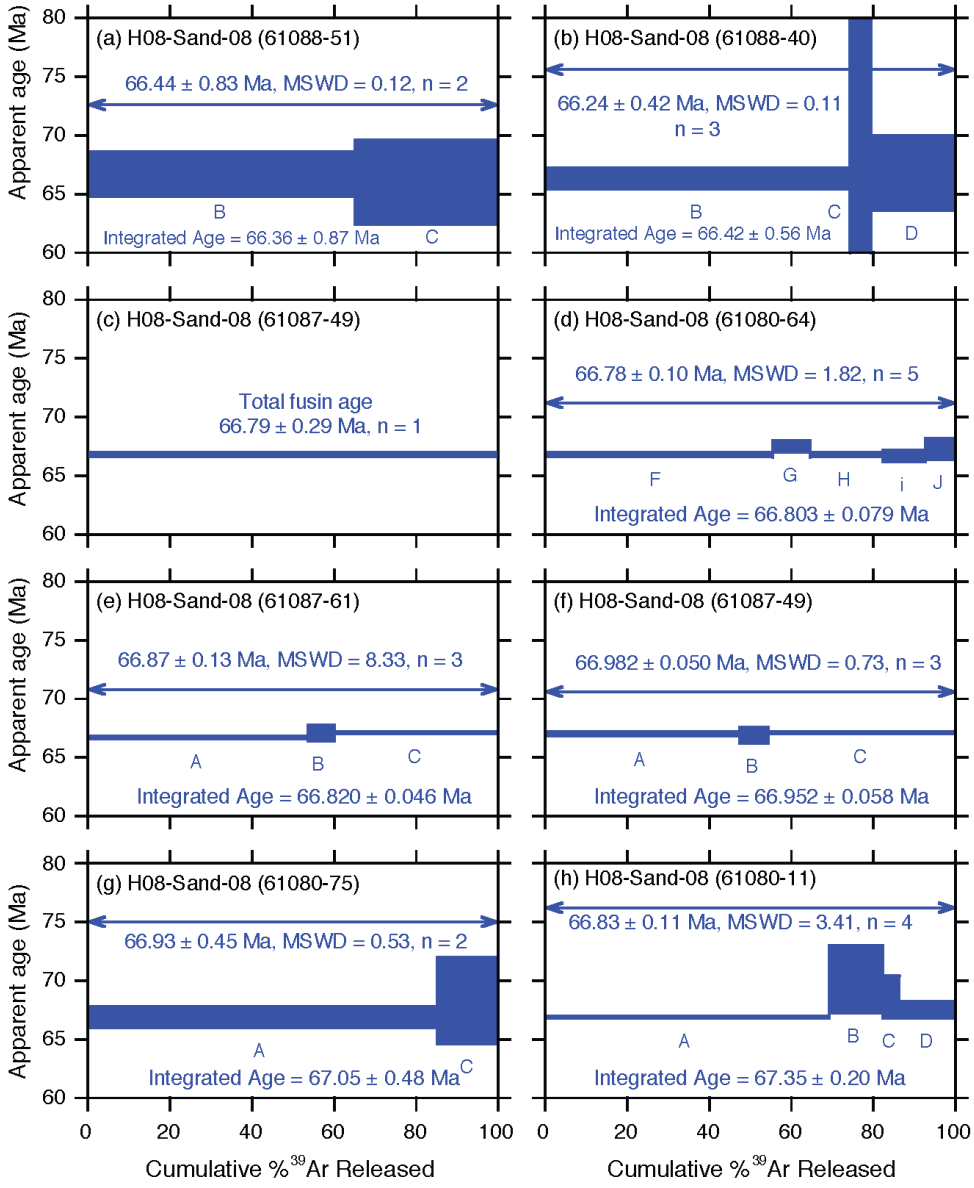

Fig. S5. Single crystal age spectra for detrital sanidine grains defining the maximum depositional age of sample H08-Sand-08. The plateau-style spectra demonstrate that the crystal dates are robust and that there is no measurable post-depositional argon loss. Note that panel 'c' is shown as an age spectrum but is a total fusion experiment rather than a step-heating experiment.

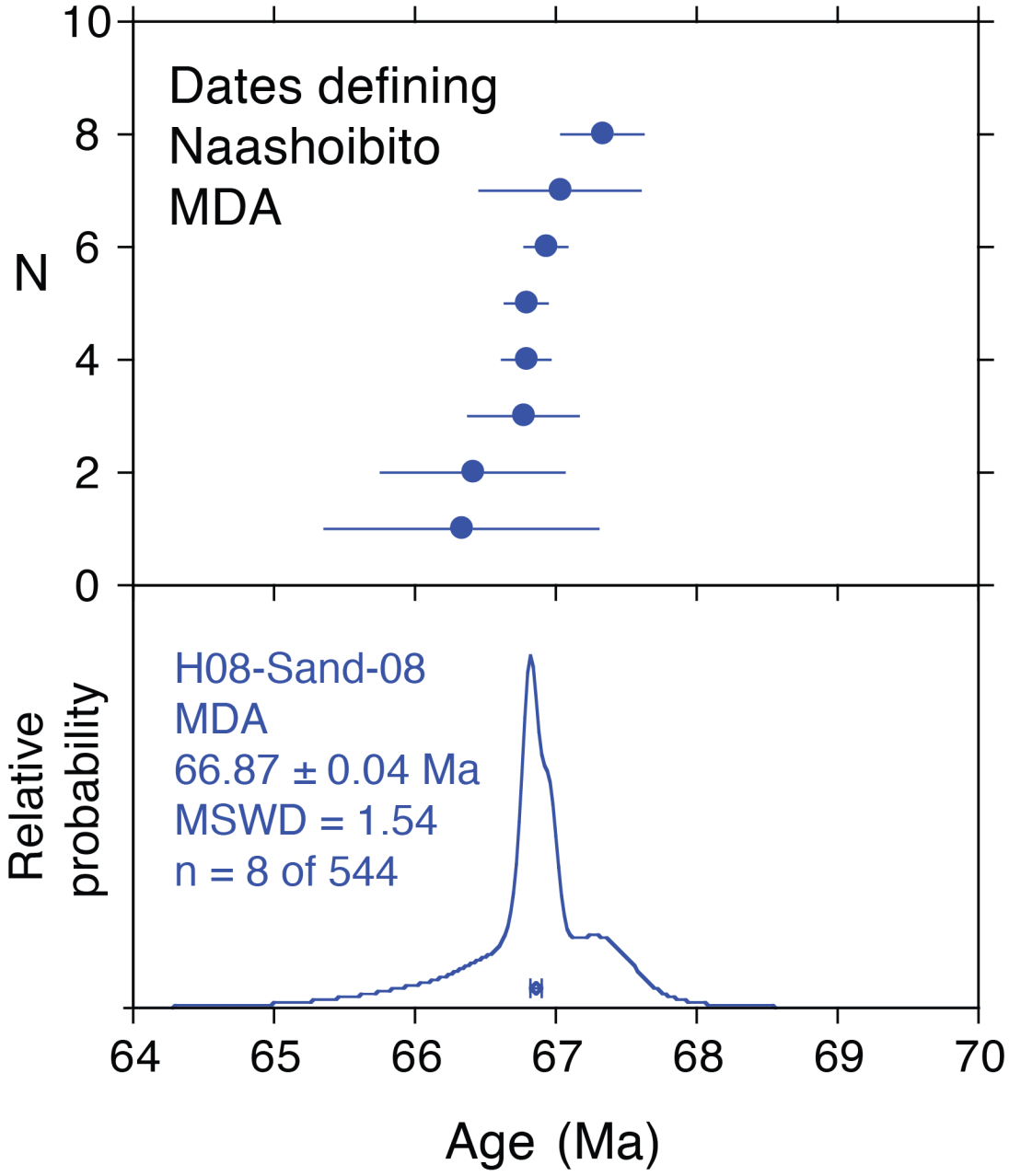

Fig. S6. Age probability distribution diagram of the eight detrital sanidine analyses used to define the MDA of sample H08-Sand-08. Error is 1σ and represents the full analytical error only.

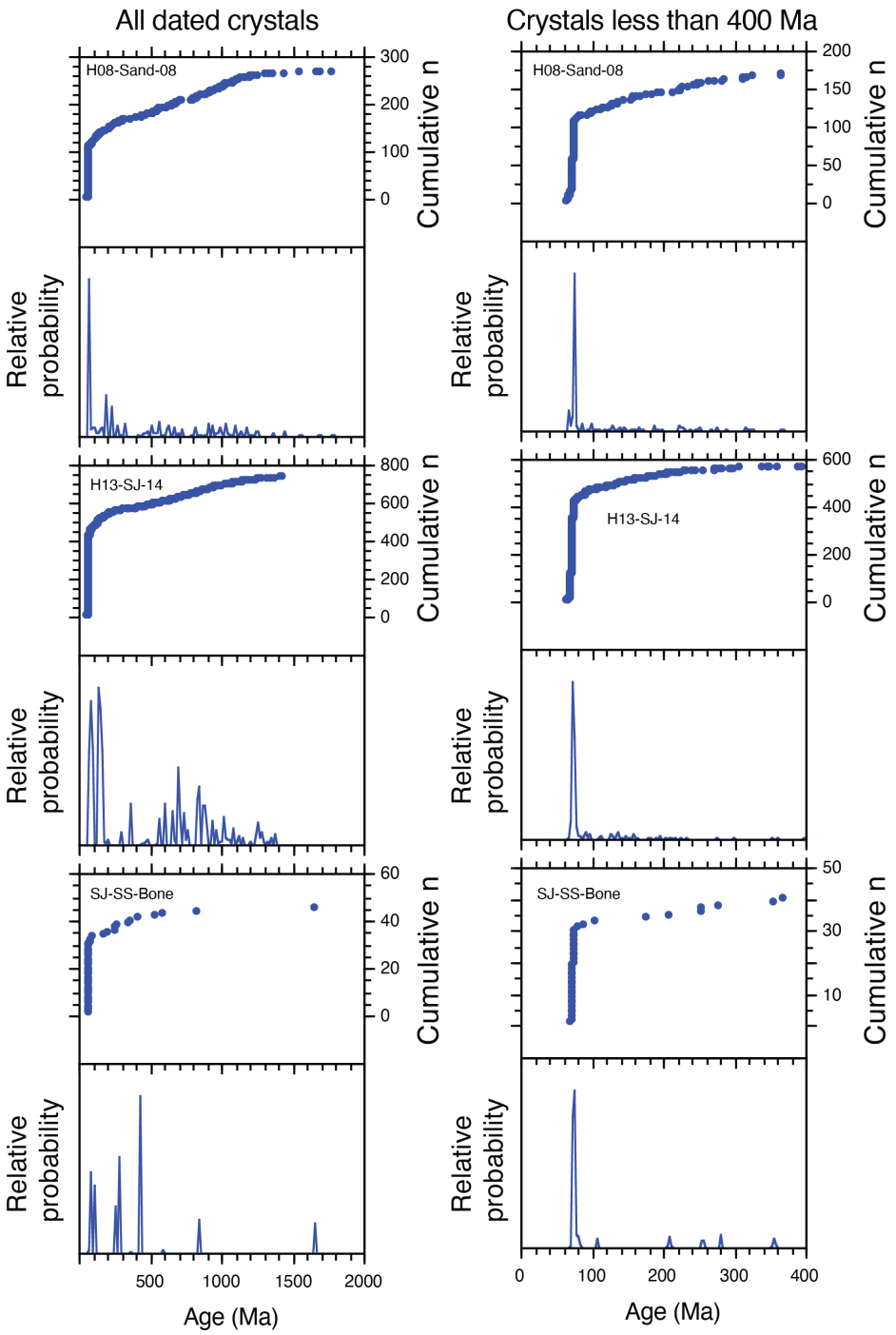

Fig. S7. Age probability distribution diagrams for the detrital sanidine dates of the three samples analyzed from the Naashoibito Formation. The left-hand panel shows all of the analyses, whereas the right-hand panel shows dates younger than 400 Ma. Because clear K-feldspar grains were viewed and chosen in air using a binocular microscope without the aid of a polarizing microscope for irradiations NM-248, NM-254 and NM-265 many chosen grains were clear microcline and orthoclase. These grains are likely represented by ages older than ca. 300 Ma. For NM-335 grains were chosen with the aid of immersion in wintergreen oil, and a polarizing microscope and thus the success rate of choosing sanidine was much higher.

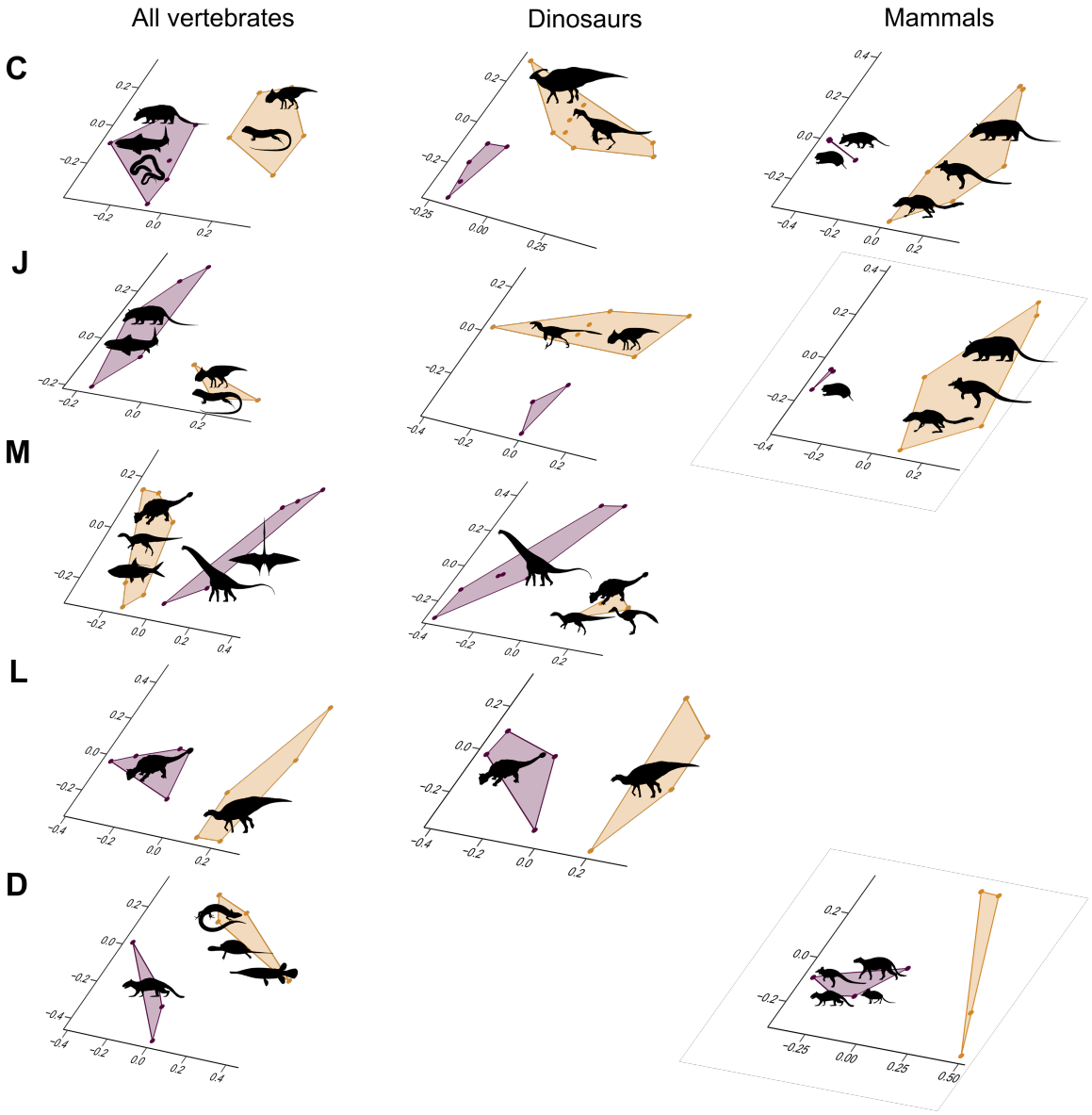

Fig. S8. Ordination plots obtained from *k*-means partitioning on residual eigenvectors delineating bioprovinces for terrestrial and fluvio-lacustrine vertebrates across the Campanian (C), Judithian (J), Maastrichtian (M), Lancian (L), Danian (D) of Laramidia. Models were also stratified for dinosaur and mammal assemblages separately. Hypothesized faunal provinces are defined in Tables S12 and S13, and silhouettes of some representative animals for each bioprovince follow Tables S24 and S25. The application of the sum of squared distance method and *k*-means partitioning suggested weak to non-existent discrete biogeographical separation in mammals inhabiting the latest Cretaceous Western Interior Basin (Table S12 and S13). Their spatial distribution in Fig. 3 was plotted on paleocoordinates on a paleogeography of North America using the 'palaeorotate' function of the palaeoverse R package (*91*) and rgplates (*144*)

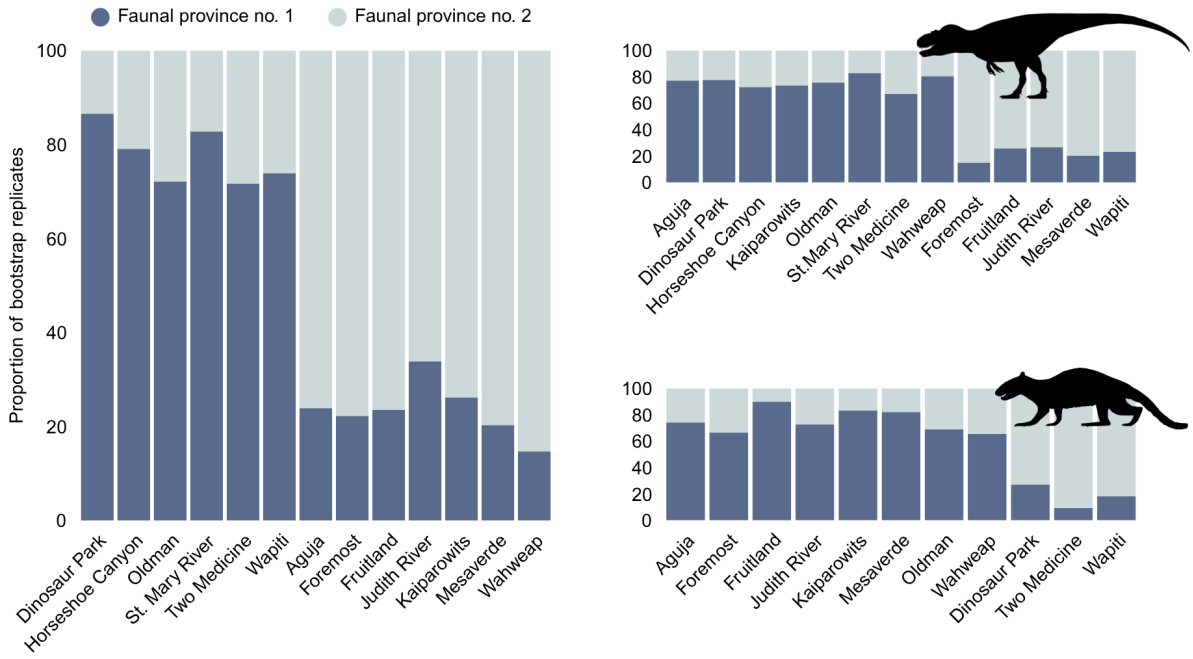

Fig. S9. Results of sensitivity analysis testing the accuracy of bioprovince delineation for terrestrial and fluvio-lacustrine vertebrates during the Campanian of North America. Bar plots represent bioprovince assignment frequencies for each fossil-bearing formation after a random resampling (100 bootstrap replicates) of taxa and localities. Hypothesized faunal provinces are defined in Table S12. Models were also stratified for dinosaur and mammal assemblages separately (right-hand panels).

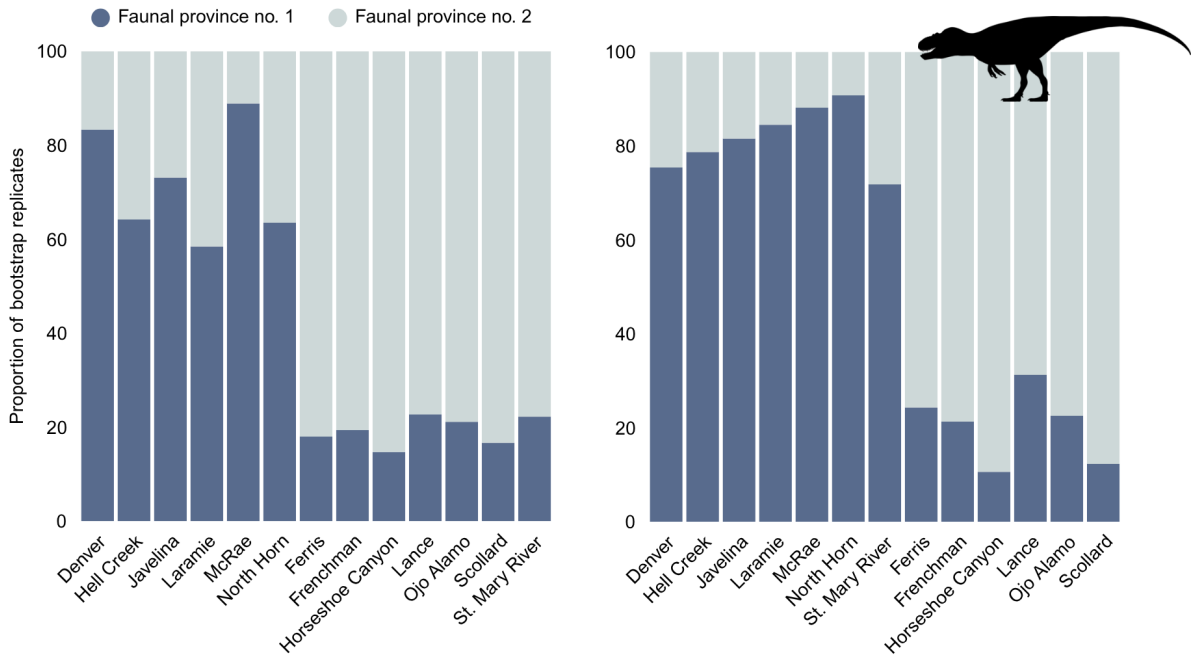

Fig. S10. Results of sensitivity analysis testing the accuracy of bioprovince delineation for terrestrial and fluvio-lacustrine vertebrates during the Maastrichtian of North America. Bar plots represent bioprovince assignment frequencies for each fossil-bearing formation after a random resampling (100 bootstrap replicates) of taxa and localities. Hypothesized faunal provinces are defined in Table S12. Models were also stratified for dinosaur assemblages separately (right-hand panel). The application of the sum of squared distance method and *k*-means partitioning suggested weak to non-existent discrete biogeographical separation in mammals inhabiting Laramidian ecosystems during the terminal Cretaceous.

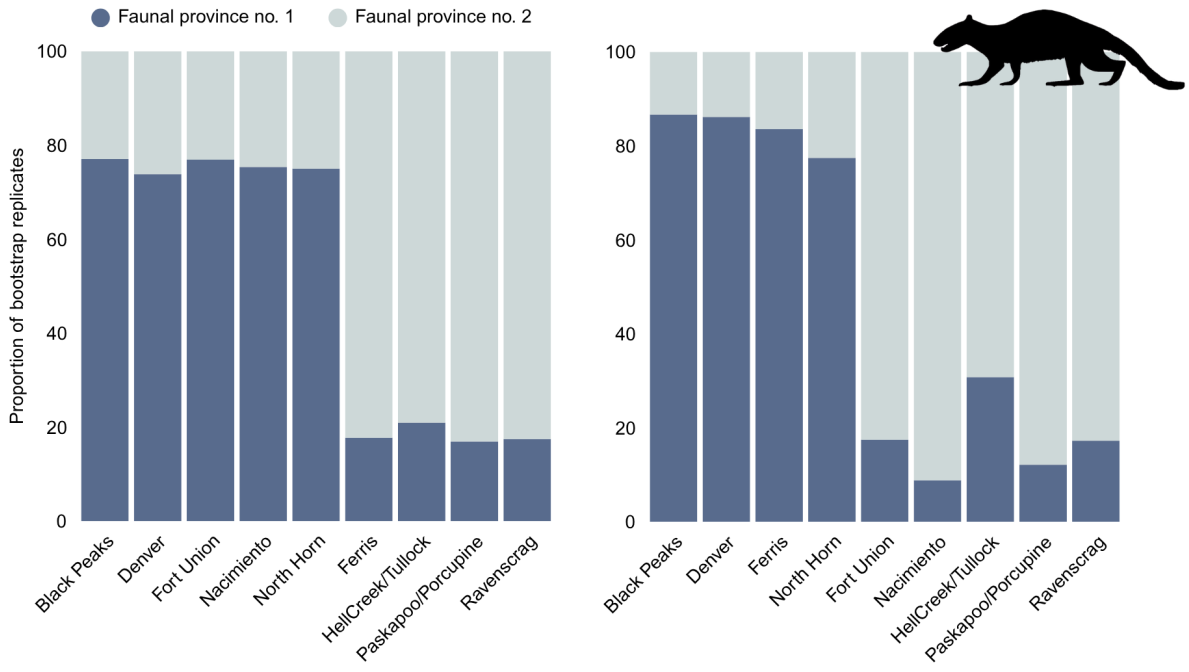

Fig. S11. Results of sensitivity analysis testing the accuracy of bioprovince delineation for terrestrial and fluvio-lacustrine vertebrates across the early Paleogene Laramidia. Bar plots represent bioprovince assignment frequencies for each fossil-bearing formation after a random resampling (100 bootstrap replicates) of taxa and localities. Hypothesized faunal provinces are defined in Table S12. Models were also stratified for mammal assemblages separately (right-hand panel).

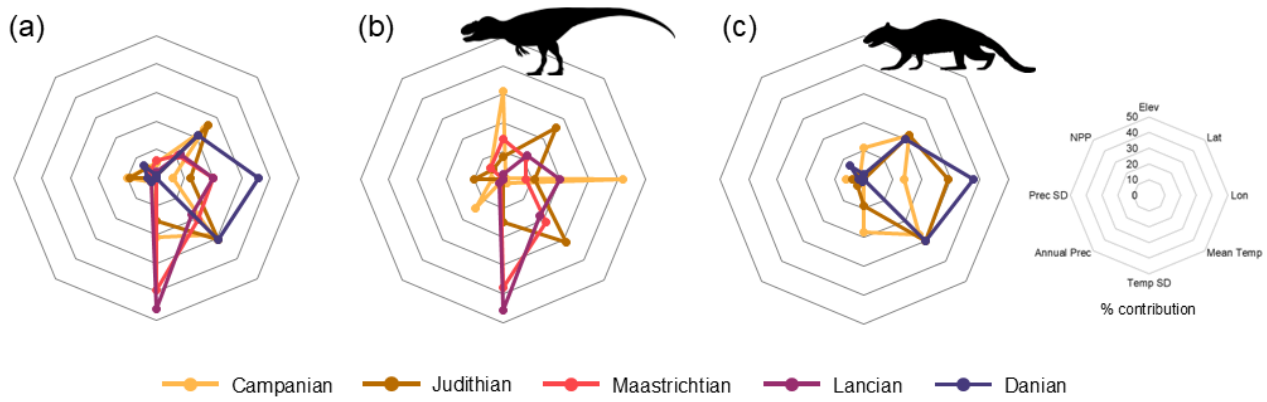

Fig. S12. Relative contributions (%) of different paleoenvironmental variables to faunal provinciality across the Upper Cretaceous and early Paleogene Laramidia. These results are based on discriminant analysis of principal components (DAPC) on residual eigenvectors (Figure S8) and hypothesized faunal provinces (Tables S12−S13) for **(a)** all terrestrial and fluvio-lacustrine vertebrates, as well as for **(b)** dinosaur and **(c)** mammal assemblages separately. Note that the application of the sum of squared distance method and *k*-means partitioning suggested weak to non-existent discrete biogeographical separation in latest Cretaceous mammals (Tables S12−S13). *Elev*, elevation (*m*); *Lat*, paleolatitude (º); *Lon*, paleolongitude (º); *Mean Temp*, near-surface (1.5 m) mean annual temperature (*ºC*); *Temp SD*, near-surface (1.5 m) annual temperature SD (*ºC*); *Annual Prec*, annual average precipitation (*mm*); *Prec SD*, annual precipitation SD (*mm*); and *NPP*, net primary productivity ($g\ C\ m^{-2}\ year^{-1}$).

Table S12. Hypothesized bioprovinces for terrestrial and fluvio-lacustrine vertebrate faunas across multiple age-level time bins from the Upper Cretaceous and early Paleogene of North America. The optimal number of bioprovinces was estimated with the sum of squared distances (*115*), and we clustered assemblages for each time interval using *k*-means partitioning on residual eigenvectors (for details, *Statistical modelling* in the Methods section).

	Time interval	Clusters	Hypothesized faunal province no. 1	Hypothesized faunal province no. 2
All vertebrates				
	Campanian	2	Dinosaur Park, Horseshoe Canyon, Oldman, St. Mary River, Two Medicine, Wapiti	Aguja, Foremost, Fruitland, Judith River, Kaiparowits, Mesaverde, Wahweap
	Maastrichtian	2	Denver, Hell Creek, Javelina, Laramie, McRae, North Horn	Ferris, Frenchman, Horseshoe Canyon, Lance, Ojo Alamo, Scollard, St. Mary River
	Danian	2	Black Peaks, Denver, Fort Union, Nacimiento, North Horn	Ferris, Hell Creek/Tullock, Paskapoo/Porcupine Hills, Ravenscrag
Dinosaurs				
	Campanian	2	Aguja, Dinosaur Park, Horseshoe Canyon, Kaiparowits, Oldman, St. Mary River, Two Medicine, Wahweap	Foremost, Fruitland, Judith River, Mesaverde, Wapiti
	Maastrichtian	2	Denver, Hell Creek, Javelina, Laramie, McRae, North Horn, St. Mary River	Ferris, Frenchman, Horseshoe Canyon, Lance, Ojo Alamo, Scollard
Mammals				
	Campanian	2	Aguja, Foremost, Fruitland, Judith River, Kaiparowits, Mesaverde, Oldman, Wahweap	Dinosaur Park, Two Medicine, Wapiti
	Maastrichtian	—	—	—
	Danian	2	Black Peaks, Denver, Ferris, North Horn	Fort Union, Nacimiento, Hell Creek/Tullock, Paskapoo/Porcupine Hills, Ravenscrag

The application of the sum of squared distance method on *k*-means partitioning suggested weak to non-existent discrete biogeographical separation in mammalian faunas inhabiting the end-Cretaceous Laramidia.

Table S13. Hypothesized bioprovinces for terrestrial and fluvio-lacustrine vertebrate faunas across different faunal stages from the Upper Cretaceous of North America (sensitivity test at finer temporal resolution of NALMAs, see *Statistical modelling* in the Methods section). The optimal number of bioprovinces was estimated with the sum of squared distances (*115*), and we clustered assemblages for each time interval using *k*-means partitioning on residual eigenvectors. Note that we have tested for bioprovinces using two versions of the Judithian dataset: one with and the other without the Mesaverde formation, due to uncertainty regarding its precise age (see references in SI datasets).

	Time interval	Clusters	Hypothesized faunal province no. 1	Hypothesized faunal province no. 2
All vertebrates				
	Judithian	2	Dinosaur Park, Oldman, Two Medicine, Wapiti	Aguja, Foremost, Fruitland, Judith River, Kaiparowits
	Judithian (incl. Mesaverde Fm.)	2	Dinosaur Park, Oldman, Two Medicine, Wapiti	Aguja, Foremost, Fruitland, Judith River, Kaiparowits, Mesaverde
	Lancian	2	Denver, Hell Creek, Javelina, Laramie, North Horn	Ferris, Frenchman, Lance, Ojo Alamo, Scollard
Dinosaurs				
	Judithian	2	Dinosaur Park, Foremost, Fruitland, Oldman, Two Medicine, Wapiti	Aguja, Judith River, Kaiparowits
	Judithian (incl. Mesaverde Fm.)	2	Dinosaur Park, Foremost, Fruitland, Oldman, Two Medicine, Wapiti	Aguja, Judith River, Kaiparowits, Mesaverde
	Lancian	2	Denver, Hell Creek, Javelina, Laramie, North Horn	Ferris, Frenchman, Lance, Ojo Alamo, Scollard
Mammals				
	Judithian	2	Aguja, Foremost, Fruitland, Judith River, Kaiparowits, Oldman	Dinosaur Park, Two Medicine, Wapiti
	Judithian (incl. Mesaverde Fm.)	2	Aguja, Foremost, Fruitland, Judith River, Kaiparowits, Mesaverde. Oldman	Dinosaur Park, Two Medicine, Wapiti
	Lancian	—	—	—

The application of the sum of squared distance method on *k*-means partitioning suggested weak to non-existent discrete biogeographical separation in mammalian faunas during the Lancian biozone of Laramidia.

Table S14. Number and structure of hypothesized bioprovinces for terrestrial and fluvio-lacustrine vertebrate faunas after accounting for the effect of formations spanning multiple stratigraphic ranges across the Upper Cretaceous of North America. The optimal number of bioprovinces was estimated with the sum of squared distances (*115*), and we clustered assemblages for each time interval using *k*-means partitioning on residual eigenvectors (for details, see *Statistical modelling* in the Methods section).

Time interval	Clusters	Hypothesized faunal province no. 1	Hypothesized faunal province no. 2
Campanian (excl. Horseshoe Canyon Fm.)	2	Dinosaur Park, Oldman, St. Mary River, Two Medicine, Wapiti	Aguja, Foremost, Fruitland, Judith River, Kaiparowits, Mesaverde, Wahweap
Campanian (excl. Mesaverde Fm.)	2	Dinosaur Park, Horseshoe Canyon, Oldman, St. Mary River, Two Medicine, Wapiti	Aguja, Foremost, Fruitland, Judith River, Kaiparowits, Wahweap
Campanian (excl. St. Mary River Fm.)	2	Dinosaur Park, Horseshoe Canyon, Oldman, Two Medicine, Wapiti	Aguja, Foremost, Fruitland, Judith River, Kaiparowits, Mesaverde, Wahweap
Campanian (excl. Wapiti Fm.)		Dinosaur Park, Horseshoe Canyon, Oldman, St. Mary River, Two Medicine	Aguja, Foremost, Fruitland, Judith River, Kaiparowits, Mesaverde, Wahweap
Maastrichtian (excl. Horseshoe Canyon Fm.)	2	Denver, Hell Creek, Javelina, McRae, North Horn	Ferris, Frenchman, Lance, Laramie, Ojo Alamo, Scollard, St. Mary River
Maastrichtian (excl. St. Mary River Fm.)	2	Denver, Hell Creek, Javelina, Laramie, McRae, North Horn	Ferris, Frenchman, Horseshoe Canyon, Lance, Ojo Alamo, Scollard

Table S15. Number and structure of hypothesized bioprovinces for dinosaurian faunas after accounting for the effect of formations spanning multiple stratigraphic ranges across the Upper Cretaceous of North America. The optimal number of bioprovinces was estimated with the sum of squared distances (*115*), and we clustered assemblages for each time interval using *k*-means partitioning on residual eigenvectors (for details, see *Statistical modelling* in the Methods section).

Time interval	Clusters	Hypothesized faunal province no. 1	Hypothesized faunal province no. 2
Campanian (excl. Horseshoe Canyon Fm.)	2	Aguja, Dinosaur Park, Kaiparowits, Oldman, St. Mary River, Two Medicine, Wahweap	Foremost, Fruitland, Judith River, Mesaverde, Wapiti
Campanian (excl. Mesaverde Fm.)	2	Aguja, Dinosaur Park, Horseshoe Canyon, Kaiparowits, Oldman, St. Mary River, Wahweap	Foremost, Fruitland, Judith River, Two Medicine, Wapiti
Campanian (excl. St. Mary River Fm.)	2	Aguja, Dinosaur Park, Horseshoe Canyon, Kaiparowits, Oldman, Wahweap	Foremost, Fruitland, Judith River, Mesaverde, Oldman, Two Medicine, Wapiti
Campanian (excl. Wapiti Fm.)	2	Aguja, Dinosaur Park, Horseshoe Canyon, Kaiparowits, Oldman, St. Mary River, Two Medicine, Wahweap	Foremost, Fruitland, Judith River, Mesaverde
Maastrichtian (excl. Horseshoe Canyon Fm.)	2	Denver, Hell Creek, Javelina, Laramie, McRae, North Horn, St. Mary River	Ferris, Frenchman, Lance, Ojo Alamo, Scollard
Maastrichtian (excl. St. Mary River Fm.)	2	Denver, Hell Creek, Javelina, Laramie, McRae, North Horn	Ferris, Frenchman, Horseshoe Canyon, Lance, Ojo Alamo, Scollard

Table S16. Results of permutational multivariate analysis of variance (PERMANOVA) explaining mean average differences in the assemblage composition of hypothesized bioprovinces for terrestrial and fluvio-lacustrine vertebrates inhabiting the Upper Cretaceous and early Paleogene ecosystems of Laramidia (Table S12). Significant values are given in bold font (**$p \leq 0.01$; ***$p \leq 0.001$).

	Time interval	Sum of squares	R^2	Pseudo-*F*
All vertebrates				
	Campanian	0.57	0.16	**2.12****
	Maastrichtian	0.69	0.16	**2.05*****
	Danian	0.48	0.21	**1.86****
Dinosaurs				
	Campanian	0.57	0.17	**2.29*****
	Maastrichtian	0.80	0.20	**2.78*****
Mammals				
	Campanian	0.81	0.27	**3.37****
	Maastrichtian	—	—	—
	Danian	0.66	0.29	**2.85****

Note that the case for provinciality of terminal Cretaceous mammals is weak to non-existent across the Western Interior Basin (Table S12).

Table S17. Results of permutational multivariate analysis of variance (PERMANOVA) explaining mean average differences in the assemblage composition of hypothesized bioprovinces for terrestrial and fluvio-lacustrine vertebrates across different faunal stages from the Upper Cretaceous of North America (Table S13). Significant values are given in bold font (***p* ≤ 0.05; ****p* ≤ 0.01).

	Time interval	Sum of squares	R^2	Pseudo-*F*
All vertebrates				
	Judithian	0.42	0.22	**1.93****
	Judithian (incl. Mesaverde)	0.47	0.18	**1.96****
	Lancian	0.57	0.18	**1.75***
Dinosaurs				
	Judithian	0.35	0.21	**1.83***
	Judithian (incl. Mesaverde)	0.43	0.17	**1.89***
	Lancian	0.69	0.24	**2.48***
Mammals				
	Judithian	0.71	0.33	**3.40****
	Judithian (incl. Mesaverde)	0.83	0.27	**3.41****
	Lancian	—	—	—

Note that the case for provinciality of Lancian mammals is weak to non-existent across the Western Interior Basin (Table S13).

Table S18. Results of permutational multivariate analysis of variance (PERMANOVA) explaining mean average differences in the assemblage composition of hypothesized bioprovinces for terrestrial and fluvio-lacustrine vertebrates after accounting for the effect of formations spanning multiple stratigraphic boundaries across the Upper Cretaceous of North America (Table S14). Significant values are given in bold font (**$p \leq 0.01$; ***$p \leq 0.001$).

Time interval	Sum of squares	R^2	Pseudo-*F*
Campanian (excl. Horseshoe Canyon Fm.)	0.51	0.16	**1.95*** **
Campanian (excl. Mesaverde Fm.)	0.50	0.16	**1.88** **
Campanian (excl. St. Mary River Fm.)	0.53	0.17	**2.06** **
Campanian (excl. Wapiti Fm.)	0.54	0.17	**2.06** **
Maastrichtian (excl. Horseshoe Canyon Fm.)	0.67	0.17	**1.99** **
Maastrichtian (excl. St. Mary River Fm.)	0.69	0.17	**2.06*** **

Table S19. Results of permutational multivariate analysis of variance (PERMANOVA) explaining mean average differences in dinosaur assemblage composition after accounting for the effect of formations spanning multiple stratigraphic boundaries across the Upper Cretaceous of North America (Table S15). Significant values are given in bold font (***p* ≤ 0.05; ****p* ≤ 0.01; *****p* ≤ 0.001).

Time interval	Sum of squares	R^2	Pseudo-*F*
Campanian (excl. Horseshoe Canyon Fm.)	0.52	0.18	**2.14***
Campanian (excl. Mesaverde Fm.)	0.51	0.18	**2.16*****
Campanian (excl. St. Mary River Fm.)	0.48	0.17	**2.10****
Campanian (excl. Wapiti Fm.)	0.50	0.17	**2.04*****
Maastrichtian (excl. Horseshoe Canyon Fm.)	0.76	0.21	**2.72*****
Maastrichtian (excl. St. Mary River Fm.)	0.81	0.22	**2.88*****

Table S20. Results for the tests of homogeneity of multivariate dispersion (PERMDISP) exploring differences in overall beta diversity between hypothesized bioprovinces for terrestrial and fluvio-lacustrine vertebrates inhabiting the Upper Cretaceous and early Paleogene Laramidia (Table S12). *F*-values and *p*-values were obtained from tests for differences in multivariate dispersion using 999 permutations of least-squares residuals. Significant values are given in bold font (*****$p \leq 0.001$**).

	Time interval	Sum of squares	R^2	*F* (*p*-value)
All vertebrates				
	Campanian	0.00	0.00	0.06 (0.79)
	Maastrichtian	0.00	0.00	0.12 (0.86)
	Danian	0.01	0.01	7.76 (0.07)
Dinosaurs				
	Campanian	0.00	0.00	0.04 (0.85)
	Maastrichtian	0.00	0.00	0.02 (0.92)
Mammals				
	Campanian	0.12	0.12	**17.64*****
	Maastrichtian	—	—	—
	Danian	0.00	0.00	0.05 (0.83)

Note that the case for provinciality of terminal Cretaceous mammals is weak to non-existent across the Western Interior Basin (Table S12).

Table S21. Results for the tests of homogeneity of multivariate dispersion (PERMDISP) exploring differences in overall beta diversity between hypothesized bioprovinces for terrestrial and fluvio-lacustrine vertebrates across different faunal stages from the Upper Cretaceous of North America (Table S13). *F*-values and *p*-values were obtained from tests for differences in multivariate dispersion using 999 permutations of least-squares residuals. Significant values are given in bold font (**$\boldsymbol{**p \leq 0.01}$; **$\boldsymbol{***p \leq 0.001}$).

	Time interval	Sum of squares	R^2	*F* (*p*-value)
All vertebrates				
	Judithian	0.02	0.02	7.77 (0.04)
	Judithian (incl. Mesaverde)	0.01	0.01	2.77 (0.13)
	Lancian	0.00	0.00	0,04 (0.97)
Dinosaurs				
	Judithian	0.00	0.00	0.17 (0.68)
	Judithian (incl. Mesaverde)	0.00	0.00	0.04 (0.89)
	Lancian	0.00	0.00	0.01 (0.95)
Mammals				
	Judithian	0.14	0.14	**23.30*****
	Judithian (incl. Mesaverde)	0.11	0.11	**14.51****
	Lancian	—	—	—

Note that the case for provinciality of terminal Cretaceous mammals is weak to non-existent across the Western Interior Basin (Table S13).

Table S22. Results for the tests of homogeneity of multivariate dispersion (PERMDISP) exploring differences in overall beta diversity between hypothesized bioprovinces for terrestrial and fluvio-lacustrine vertebrates after accounting for the effect of formations spanning multiple stratigraphic boundaries across the Upper Cretaceous of North America (Table S14). *F*-values and *p*-values were obtained from tests for differences in multivariate dispersion using 999 permutations of least-squares residuals.

Time interval	Sum of squares	R^2	*F* (*p*-value)
Campanian (excl. Horseshoe Canyon Fm.)	0.00	0.00	0.71 (0.42)
Campanian (excl. Mesaverde Fm.)	0.00	0.00	0.06 (0.84)
Campanian (excl. St. Mary River Fm.)	0.00	0.00	0.11 (0.77)
Campanian (excl. Wapiti Fm.)	0.00	0.00	0.59 (0.46)
Maastrichtian (excl. Horseshoe Canyon Fm.)	0.01	0.01	1.25 (0.32)
Maastrichtian (excl. St. Mary River Fm.)	0.00	0.00	0.05 (0.95)

Table S23. Results for the tests of homogeneity of multivariate dispersion (PERMDISP) exploring differences in overall beta diversity between hypothesized bioprovinces for dinosaurian faunas after accounting for the effect of formations spanning multiple stratigraphic boundaries across the Upper Cretaceous of North America (Table S15). *F*-values and *p*-values were obtained from tests for differences in multivariate dispersion using 999 permutations of least-squares residuals.

Time interval	Sum of squares	R^2	*F* (*p*-value)
Campanian (excl. Horseshoe Canyon Fm.)	0.00	0.00	0.15 (0.80)
Campanian (excl. Mesaverde Fm.)	0.00	0.00	0.09 (0.75)
Campanian (excl. St. Mary River Fm.)	0.00	0.00	0.45 (0.51)
Campanian (excl. Wapiti Fm.)	0.00	0.00	0.22 (0.64)
Maastrichtian (excl. Horseshoe Canyon Fm.)	0.00	0.00	0.04 (0.92)
Maastrichtian (excl. St. Mary River Fm.)	0.00	0.00	0.17 (0.75)

Table S24. Results of indicator species analysis (α-level = 0.05, 999 permutations) identifying target taxa of hypothesized bioprovinces for terrestrial and fluvio-lacustrine vertebrates inhabiting the Upper Cretaceous and early Paleogene ecosystems of Laramidia. For each taxon, we include the indicator value index (IndVal ≥ 0.5) and the statistical significance of the association (bolded if ***p*-value ≤ 0.05 or ****p*-value ≤ 0.01). Discrete faunal provinces are defined in Table S12.

	Time interval	Hypothesized faunal province no. 1	Hypothesized faunal province no. 2
All vertebrates			
	Campanian	**Leptoceratopsidae (0.71*)**, **Teiidae (0.71*)**, Albertosaurinae (0.68), Gonorynchiformes (0.58), Microraptoria (0.58), Osteoglossomorpha (0.58)	**Alphadontidae (0.93**)**, **Hybodontiformes (0.85*)**, Adocidae (0.79), Albuliformes (0.79), Scincomorpha (0.79), **Alethinophidia (0.76*)**, Picopsidae (0.66), Leptictida (0.56), Orectolobiformes (0.56), Zhelestidae (0.56), Crocodylomorpha (0.54), Helochelydridae (0.54)
	Maastrichtian	Titanosauria (0.62), Azhdarchidae (0.58)	**Ankylosauridae (0.85*)**, Ornithomimidae (0.79), Scincomorpha (0.79), Choristodera (0.76), **Elopiformes (0.76*)**, **Thescelosauridae (0.76*)**, Troodontidae (0.76), Alphadontidae (0.67), Aspidorhynchiformes (0.67), Nanhsiungchelyidae (0.67), Pachycephalosauridae (0.67), Acipenseriformes (0.56), Adocidae (0.56), Albuliformes (0.56), Cimolesta (0.56), Cimolomyidae (0.56), Compsemydidae (0.56), Esociformes (0.56), Leptictida (0.56), Leptoceratopsidae (0.56), Pediomyoidea (0.56), Plastomenidae (0.56), Stagodontidae (0.56)
	Danian	**Anguimorpha (1.00**)**, **Lepisosteiformes (1.00**)**, **Compsemydidae (0.89*)**, **Trionychidae (0.89*)**, Adocidae (0.78), Baenidae (0.78), Conoryctidae (0.78), Dermatemydidae (0.78), Amphisbaenia (0.63), Pentacodontidae (0.63)	Cimolesta (0.85), Dermoptera (0.60), Albanerpetontidae (0.50)
Dinosaurs			
	Campanian	**Lambeosaurinae (0.84*)**, **Caenagnathidae (0.79)**, Leptoceratopsidae (0.61), Microraptoria (0.50)	No indicator taxa with IndVal greater than 0.5

Continues

	Time interval	Hypothesized faunal province no. 1	Hypothesized faunal province no. 2
	Maastrichtian	Titanosauria (0.56)	**Ankylosauridae (0.94**)**, **Thescelosauridae (0.84*)**, **Troodontidae (0.84*)**, Pachycephalosauridae (0.74), Lambeosaurinae (0.58)
Mammals			
	Campanian	**Alphadontidae (1.00**)**, Leptictida (0.71), Zhelestidae (0.71), Picopsidae (0.61)	Didelphimorphia (0.82), Spalacotheriidae (0.58)
	Maastrichtian	—	—
	Danian	No indicator taxa with IndVal greater than 0.5	**Leptictida (0.89*)**, **Macroscelidea (0.89*)**, **Pantodonta (0.89*)**, **Phenacodontidae (0.89*)**, Dermoptera (0.78), Eulipotyphla (0.78), Palaeoryctidae (0.78), Pantolestidae (0.78), Pentacodontidae (0.63)

Note that the case for provinciality of terminal Cretaceous mammals is weak to non-existent across the Western Interior Basin (Table S14).

Table S25. Results of indicator species analysis (α-level = 0.05, 999 permutations) identifying target taxa of hypothesized bioprovinces for terrestrial and fluvio-lacustrine vertebrates across different faunal stages from the Upper Cretaceous of North America. For each taxon, we include the indicator value index (IndVal ≥ 0.5) and the statistical significance of the association (bolded if ***p*-value ≤ 0.05 or ****p*-value ≤ 0.01). Discrete faunal provinces are defined in Table S13.

	Time interval	Hypothesized faunal province no. 1	Hypothesized faunal province no. 2
All vertebrates			
	Judithian	**Leptoceratopsidae (0.87*)**, **Teiidae (0.87*)**, Didelphimorphia (0.85), Gonorynchiformes (0.71), Microraptoria (0.71), Osteoglossomorpha (0.71), Xenosauridae (0.60)	**Alphadontidae (0.90*)**, **Hybodontiformes (0.78*)**, Picopsidae (0.66), Alethinophidia (0.63)
	Lancian	Saurolophinae (0.67)	**Ankylosauridae (0.91*)**, Scincomorpha (0.84), Alphadontidae (0.80), Multituberculata (0.80), Pachycephalosauridae (0.80), Thescelosauridae (0.80), Troodontidae (0.80), Elopiformes (0.78), Adocidae (0.67), Choristodera (0.67), Cimolesta (0.67), Cimolomyidae (0.67), Compsemydidae (0.67), Leptictida (0.67), Nanhsiungchelyidae (0.67), Plastomenidae (0.67), Richardoestesia (0.67)
Dinosaurs			
	Judithian	Dromaeosaurinae (0.82), Leptoceratopsidae (0.71), Microraptoria (0.58)	No indicator taxa with IndVal greater than 0.5
	Lancian	Saurolophinae (0.67)	**Ankylosauridae (0.91*)**, Pachycephalosauridae (0.80), Thescelosauridae (0.80), Troodontidae (0.80)
Mammals			
	Judithian	**Alphadontidae (1.00**)**, Leptictida (0.82), Picopsidae (0.71), Zhelestidae (0.71)	Spalacotheriidae (0.58)
	Lancian	—	—

Note that the case for provinciality of Lancian mammals is weak to non-existent across the Western Interior Basin (Table S13).